Quantum interfaces between atomic and solid state systems

Nikos Daniilidis and Hartmut Häffner

(ΩDated:)

Abstract

We discuss interfacing trapped atomic systems with solid-state systems such as superconducting Josephson-junction devices or nanomechanical oscillators. Such hybrid quantum systems could ease scalable quantum information processing and yield novel and profound in- sight into the quantum mechanics of macroscopic quantum many- body systems. We review the relevant interactions and illuminate the role of the vastly differing impedance of atomic and solid-state systems. We give some basic guidelines toward combining quantum systems, and finally, discuss some concrete proposals to interface atomic with solid-state systems.

I. INTRODUCTION

The control of atomic systems has reached an unparalleled level. Employing laser cooling and control, such complex quantum phenomena as entanglement have been demonstrated and are well controlled both on the individual atom level [1, 2], as well as on the scale of few thousands or millions of atoms [3]. From a fundamental aspect, these are quite exciting developments, but the transfer of quantum control to technological applications is impeded by delicate engineering requirements.

At the same time, solid-state devices are the driving force for technological innovations with a broad range of applications, especially in electronics. With respect to exploiting quantum properties, superconducting devices are quite attractive [4–6]. These can be controlled very well, and recently their coherence properties have been extended almost into the 100-ms regime [7, 8].

It is tempting to merge these disparate systems into new quantum devices and to take advantage of their different features. For instance, in view of scalable quantum information processing, we envision that trapped atoms can serve as a quantum memory, while the actual processing would be carried out with an array of Josephson-junction devices. So, from a technological perspective, we can capitalize on the respective advantages of different platforms to build novel devices with improved characteristics.

From a more fundamental standpoint, such hybrid quantum systems can enable us to study collective quantum effects in condensed matter systems. To do this, one can probe the quantum mechanics in the solid state, using the sophisticated toolbox available for atomic systems. In particular, we envision preparing an atom in an interesting quantum state such as a Schrödinger cat state and then transferring this state back and forth between the atom and a complex solid-state device. Reconstructing the quantum state of the atom after this procedure will give us valuable insight into the decoherence properties of the degree of freedom the atom was coupled to and more generally into the emergent quantum mechanics of the solid state. Such systems will combine the bottom-up approach of assembling individual atoms into complex quantum devices with the top- down approach of isolating individual degrees of freedom in the solid state. The purpose of this review is to evaluate various options and to assess the difficulties in this endeavor of merging quantum systems. We choose to cover a relatively wide variety of physical systems at the expense of

providing detail for each.

We concentrate on interfacing individual degrees of freedom of trapped atoms or ions on one side, with collective degrees of freedom of solid-state devices such as Josephson-junction devices and nanomechanical oscillators. We focus on the electromagnetic interactions of atoms, mainly with electrical circuits, and mention briefly the coupling to mechanical systems. Superconducting devices are currently the most advanced solid-state platform for quantum information processing. Nanomechanical oscillators, however, are straightforward to couple to and are promising as transducers. They were recently reviewed by Hunger *et al.* [9]. We do not discuss here interfacing atoms to other solid-state systems such as nitrogen-vacancy (NV) centers in diamond or semiconductor devices such as quantum dots, despite the interesting physics involved.

Often, the observation of quantum mechanical degrees of freedom in condensed matter is linked to the question of under which conditions such behavior should, in principle, be observable [10, 11]. The experimental systems required to investigate this question may need to meet different design guidelines than systems optimized for quantum information processing (9). We do not address this issue here. Instead, we take the practicing experimentalist's approach that quantum mechanical behavior is, to date, limited by technical sources of decoherence, i.e., environmental degrees of freedom that are not sufficiently controlled [12].

A. Challenges and Features

The difficulties associated with interfacing atoms with solid-state systems can hardly be over- estimated. We see challenges on both the technological and the physics side. On the technological side, trapped-atom physics methods greatly differ from the methods used in quantum control of solid-state devices. For instance, to interface a trapped ion with a Josephson-junction device, we must master quantum control via laser cooling on the ion trapping side and device fabrication, dilution refrigerator technology, and microwave electronics on the other side. Thus, each side brings already unique challenges to the table. In addition, we must not neglect that these technologies have to be made compatible with each other. Most proposals require optical access in the dilution refrigerator which, although in principle feasible, causes additional complications. We also need to be careful that the

lasers used to manipulate the ion do not heat up the interface. Another set of complications might arise from the connections of the ion trap to the outside world. Similar cases can be made for other system combinations, for instance when trying to interface neutral atoms with the solid state. Here in addition to excellent optical access, strong magnetic or optical fields, which could harm the coherence of the solid-state quantum system, are required.

The second level of challenges is connected to the basic properties of atomic and solid-state quantum systems. Two of the most striking features of single atoms are their small size and weak coupling to the environment. If trapped in free space, atoms are well separated from the bulk, enabling long coherence times that extend well beyond the minute timescale [13, 14]. However, the weak coupling to the environment makes it hard to establish strong coupling between different atoms. The situation is almost exactly the opposite for most solid-state systems [5]. The system size is typically much bigger and sometimes even macroscopic. The resulting strong dipole moments allow for strong coupling of the systems to each other but also to the environment. As a result, we often see reduced coherence times on the ms timescale. This poses the challenge that the solid-state system must be coupled to the atomic system within the coherence time of the solid-state system. This automatically implies that we need to selectively couple the relevant degree of freedom of the solid-state system more strongly to the atomic degree of freedom than to the sum of all other degrees of freedom in the solid-state environment. In other words, the signal induced in the solid- state system by the quantum fluctuations of the atomic system must be stronger than the noise within the solid-state device, and likewise for the signal and the noise induced on the atomic system. Thus, to avoid $1/f$ noise, which is quite prominent in the solid state, we have to use coupling mechanisms at high frequencies and engineer both systems such that they are immune to noise at low frequencies.

The task of having the solid-state system strongly couple to the atomic system is in many cases complicated by the somewhat small dipole moments of the atomic systems. This difficulty in interfacing quantum systems is related to impedance-matching considerations, and we discuss this aspect in more detail in Sections 3 and 4. We discuss how introducing a mediating system can, in certain cases, be viewed as an impedance-matching procedure. In analogy to other fields, we call this mediator the (quantum) bus. Such a bus can have two other advantages: If supporting a resonance, it can filter $1/f$ noise and thus protect the solid-state system. It can also physically separate the two systems and, as such, could ease

technological challenges. For instance, it could allow one to place the ion/atom trap in a 4 K environment, while operating the solid-state at dilution refrigerator temperatures.

One additional difficulty in building a hybrid device is that the atomic system might not resonate at the frequencies that are practical for solid-state applications. Such a timescale separation is not necessarily a complication. Slower dynamics can be accompanied by lower decoherence rates, and in this respect we can take advantage of different timescales of the atomic and solid-state systems. The frequency mismatch can be resolved by exploiting nonlinear effects in combination with a parametric drive, as mentioned in this context first by Heinzen & Wineland [15], and recently made more specific by Kielpinski *et al.* [16]. Finally, if we want to store quantum in- formation in the atoms, we need to switch off the coupling of the atomic degree of freedom to the solid-state system. Typically, either of the two systems is tunable and the switching can be achieved by changing the resonant frequencies. When using a bus or parametric frequency conversion, additional options appear.

B. Nomenclature

In the literature, hybrid systems often include two identical quantum systems connected via a third one, such as, for instance, two trapped ions in a single trap connected via their common vibrational modes. Here, however, we require that two quantum systems of different nature be linked with a deterministic quantum interface either via a direct coupling or via a quantum bus. Therefore, in abstract terms, a basic hybrid quantum device consists of two qubits and a quantum bus to interconnect them (see Figure 1). As a working criterion for what constitutes a hybrid, we take the requirement that the two qubits correspond to different physical realizations of a two-level system (TLS), e.g., a trapped atom and a superconducting qubit, or a superconducting qubit and an isolated NV spin.

Having this basic architecture in mind, we overview in Section 2 some of the different physical systems that are considered in hybrid device design. The list is not comprehensive, but limited to atomic and solid-state systems that have so far shown the biggest promise as quantum information platforms and to systems that have the potential to complement the already established ones. We also review the basic interactions between such systems, mainly with the aim to get a feeling for the typical strengths of different interactions, and for how these compare to the parameters of the quantum LEGO blocks. We then outline some

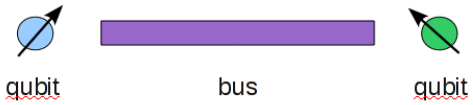

FIG. 1. A generic hybrid quantum system, consisting of two qubits and a bus to interconnect them.

basic considerations and rough rules on the importance of decoherence in hybrid devices, as well as hint to additional challenges that hybrid devices might face. Finally, we review some specific proposals that cover a wide variety of interactions and add our own estimates on what the experimental issues might be for each. The main purpose of the following discussion is to try and treat all the different possible systems on an equal footing and allow the reader to develop some intuition—thus we try to point out the common features and the differences. We hope that our approach offers useful insight and fruitful guidelines to researchers in the field seeking to evaluate existing hybrid systems or to propose new ones.

II. PHYSICAL SYSTEMS

We first give an overview of the properties of quantum systems that are usually considered as candidates for hybrid devices. We focus on their typical dipole moments, which will influence how strongly they couple to other devices, as well as the known and anticipated challenges in maximizing their coherence properties. We cover those solid-state and atomic systems that are promising due to the potential for strong interactions and long coherence times.

We start with Josephson junction–based superconducting quantum devices. The class of superconducting charge qubits (i.e., the so-called Cooper pair box and its variants) offers a solid-state realization of a TLS with promising coherence properties and very high electric dipole moments [5, 17, 18]. The energy levels of a charge qubit arise as a result of the competition between the charging energy of the island and the Josephson energy of a superconducting weak link [19]. A schematic of the basic implementation of this device is shown in Figure 2a. The variables that determine the dynamics of the charge qubit are the charge across the capacitance between the island and ground and the gauge invariant flux

across the junction. These are experimentally controlled via an externally applied voltage and an externally applied magnetic field, respectively. The circuit is usually tuned to a parameter regime where tunneling of one additional Cooper pair into the island does not result in a change of electrostatic energy. In this regime, the device can be operated at dilution refrigerator temperatures as a tunable spin, in the two-dimensional Hilbert space composed of the states $|0\rangle$, $|1\rangle$ with N and $N+1$ Cooper pairs in the island, where N is some integer (hence the name Cooper pair box) [19]. Thus, the qubit states, typically superpositions of the type $|0\rangle \pm |1\rangle$, and the transition frequency, typically in the GHz range, can be tuned by geometric design and external electric and magnetic fields. A more detailed discussion of these issues can be found in Reference 16. The dipole moment can be viewed as arising from the tunneling of a Cooper pair across a weak link between the superconducting island and the superconducting reservoir. The mean distance, d, between the island and the reservoir can range from micrometers to millimeters, giving rise to a high dipole moment that scales as $2e\,d$. The coherence properties of charge qubits have steadily improved over the past decade, due to a combination of careful engineering of the device design, and operation, and the fabrication methods, resulting in the transmon design, and more recently to the 'three-dimensional' transmon qubits [7, 8, 19**?** , 20]. Currently, energy relaxation times T_1 are up to 200 μs [7, 8, 21] (see Section 5 for a brief discussion of the terminology describing decoherence). They are thought to be limited by charge fluctuations in the dielectrics surrounding the qubit, nonequilibrium quasiparticles in the superconductor, or losses and residual photons in the microwave elements that are coupled to the qubits. The latter mechanism is also thought to limit the effective dephasing time, T_2, currently reaching 95 μs [7, 8]. An additional mechanism that can additionally limit the coherence time is critical current fluctuations in the Josephson junction.

Superconducting flux qubits consist of a SQUID loop that contains an additional inductor, as shown in Figure 2b. This circuit shows nonlinear behavior, due to the competition between the magnetic energy in the inductor, L, and the Josephson energy in the junction. It can be tuned by external magnetic fields, with typical transition frequencies also engineered to be in the GHz range. When the circuit is biased by an external magnetic field to a midpoint between integer numbers of flux quanta penetrating the loop, the different states of the circuit correspond to symmetric and antisymmetric superpositions of current running through the loop in opposite directions [19]. The magnetic moments generated by these

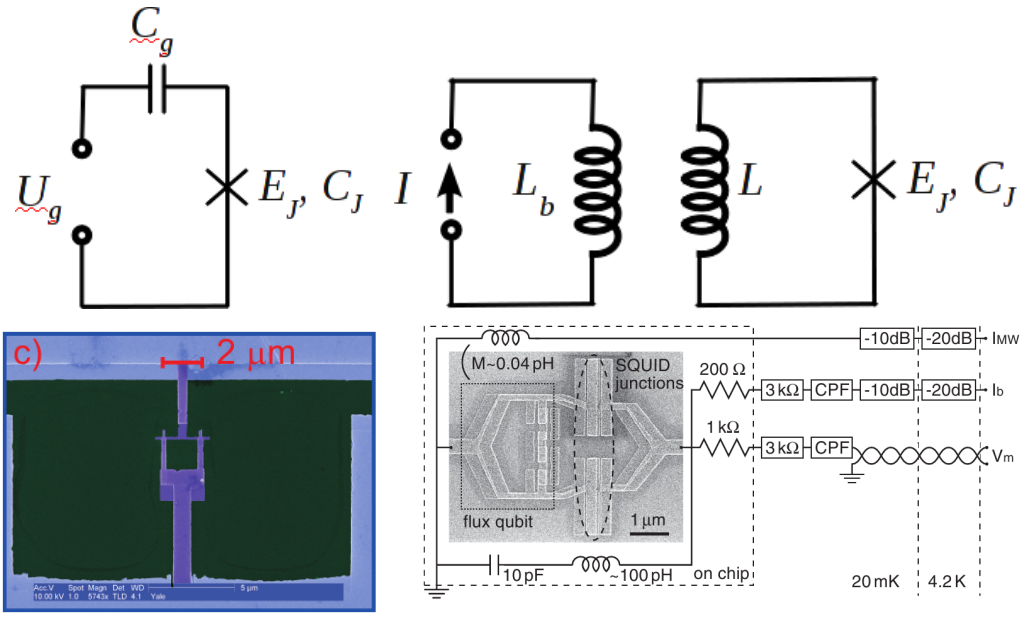

FIG. 2. (a) Schematic of a superconducting charge qubit. A Josephson junction with Josephson energy E_J, and capactiance C_J is biased by a gate voltage U_g, through a gate capacitance, C_g. (b) Schematic of a flux qubit, in which a junction is in series with an inductor, L. The flux through the loop containing the Josephson junction is controlled via an external current, I. (c) SEM picture of a superconducting charge qubit, from [22]. In this case, the qubit contains two junctions in parallel, to allow tunability with an external magnetic field. (d) SEM picture of a flux qubit, from [23]. The qubit is coupled to a SQUID for readout. The qubit flux bias is controlled via the currents I_b and $I_{\rm MW}$.

currents can be remarkable, reaching the regime of 10^{10} $\mu_{\rm B}$ for large devices with a radius of a few millemeters [24]. This implies that the flux qubit will couple magnetically to other devices or atoms. For applications where scalability and integration of the device into a complex system is desired, a limit will probably have to be placed on its physical size. Then, the magnetic moment can be viewed as being localized in space and can magnetically interact with different magnetic systems in an efficient way. As an order of magnitude estimate under these restrictions, the superconducting currents can be fractions of a μA, and the area of the loop can be several square mm, with resulting magnetic moments as high as $5 \times 10^5 \mu_{\rm B}$ [25]. Currently, the energy relaxation times are $T_1 \approx 10$ μs, but an additional source of flux noise is known to limit the dephasing time T_2. The source of this noise is thought to be fluctuating electron spins on the surfaces of the Josephson junctions in the device and is currently under investigation [26]. At the moment, the ultimate limit for the coherence time of Josephson junction–based qubits is hard to estimate, but it is expected that careful materials engineering can yield significant improvements.

There is a third class of superconducting circuits that also offers a very successful implementation of a qubit, the so-called phase qubit, which the Santa Barbara group is pursuing [27]. This device consists of a Josephson junction that is biased with a direct current close to the junction critical current. The control parameter that allows manipulations of the quantum state in this device is the current flowing through the junction. To our knowledge, there exist no proposals for coupling the phase qubit to atomic systems. Nevertheless, the general context described in the following sections could be adapted to include this kind of circuit. In particular, phase qubits are strongly coupled to on-chip electrical resonator circuits with a controllable coupling, and the methods that we overview in Sections 3 and 4 can undoubtedly provide various solutions to coupling a phase qubit to an atomic system via such a resonator. However, such a treatment is beyond the scope of this review, and here we do not deal with this circuit in more detail.

We now move on to superconducting microwave resonators that are currently used in the Josephson junction–based implementations of quantum information platforms, but they can prove useful in generic hybrid systems, as we discuss in Section 3. These can be coplanar waveguides (CPW) [17], lumped-element resonators [**?**], and—in light of recent developments in three-dimensional circuit cQED [7]—even three-dimensional microwave waveguides. The basic parameters of interest for such a resonator are the intrinsic quality factor and the characteristic impedance that can be achieved. The characteristic impedances of planar microwave resonators can vary from a few Ω [28] to kΩ if high kinetic inductance conductors are used [29]. The internal quality factor ($Q_{\rm i}$) of CPW resonators is limited by fluctuating TLSs in the interface between the superconductor and the dielectric substrate of the device [30–32]. A striking consequence of this is that $Q_{\rm i}$ decreases by one to two orders of magnitude as the temperature of the resonator decreases from liquid helium to dilution refrigerator temperatures, and as the energy stored in the resonator decreases to the few-photon level. This is a result of saturation of the TLS. In recent years, significant efforts in materials engineering have resulted in an increase of $Q_{\rm i}$ [33, 34], with values at the single-photon level currently exceeding 10^6 [35]. Moreover, it has been realized that the resonator losses can be limited by reducing the participation of the dielectric-superconductor interface in the resonant mode. One way to achieve this is by building higher characteristic impedance CPW resonators [36]. In light of the very high internal quality factors ($Q_{\rm i} > 10^7$) achieved with high kinetic inductance resonators in the 1–2 GHz range [29], it would be

very interesting to explore the possibility of further increases in quality factor at higher frequencies if this technology is employed to further reduce the effect of dielectric losses on the resonator. Finally, a very efficient way to reduce the participation of TLS in the resonant mode is to turn to three-dimensional cavity resonators [7, 8]. In these, the electric field of the resonant mode has a very small overlap with the walls of the cavity, where impurity TLS fluctuators reside, and the resulting quality factors can be very high. Quality factors higher than 10^10 [37] have been measured at 1 K in a cavity with a different geometry and for a higher frequency than the ones used in [7, 8, text].

We now move on to atomic systems. Rydberg atoms (and ions) carry rather remarkable electrical dipoles of order $n^2\, e\, a_0$, where n is the principal quantum number e the elementary charge, and a_0 the Bohr radius. This is due to the large extent of the electron orbital in highly excited states with $n \sim 50$ or more. Typical transition frequencies range from a few GHz to more than 50 GHz and can be tuned with a static electric field via Stark shifts [38, 39]. Rydberg states are long lived, with lifetimes scaling as n^3, and can thus serve as quantum memories [40]. Radiative relaxation times are in the range of 50 ms up to fractions of 1 ms for n ¿ 50 (36).50 μs up to to fractions of 1 ms for $n > 50$ [38]. The main mechanism expected to limit the coherence times of Rydberg atoms in the context of hybrid systems is electric field noise, due to the sensitivity of transition frequencies to electric fields. If the Rydberg atoms are used in the presence of biasing static electric fields, the typical sensitivity of the transition frequency to electric fields is $100\,(100/n)^2$ MHz/(V/m) [38]. We will estimate the influence of this later, in Sec. VI.

Polar molecules have dipole moments of a few Debye [41]. The degeneracy of the rotational manifold of the molecule can be broken by a dc electric field that provides a quantization axis. At the same time, the magnitude of the static field serves as a tuning knob for the molecule transition frequency due to the static Stark effect. As in the case of Rydberg atoms, this means that electric field noise will cause dephasing of the molecular state. Typical transition frequencies are in the low GHz range [42]. Besides tuning the transition, the static electric field can be used to tune the molecule to a sweet spot that is relatively insensitive to electric field variations, thus increasing the dephasing time of the molecular qubit [42]. The coherence time can be further increased by mapping the quantum information from the rotationial state of the molecule onto its internal hyperfine state. For this, one would employ a microwave field driving transition of the form $|N, F_3, m_{F_3}\rangle \leftrightarrow |N', F_3', m_{F_3}\rangle$,

where N refers to the rotational quantum number of the molecule and F_3 to the hyperfine quantum number of the molecule [42, 43].

Trapped ions can be viewed as possessing an electric dipole moment, given that they behave as point charges in a harmonic trapping potential (for a review of the quantum dynamics of trapped ions we refer to [44]). The dipole moment is proportional to the extent of the motional ground state wavefunction, and it is given by $\mu = e\,x_0 = e\sqrt{\hbar/(2\,m\omega)}$, where m is the ion mass, and ω the ion frequency in the trap. The ion frequency is adjustable in the range from a few hundred kHz to several MHz. The masses of ions used for quantum information range from 9–200 amu. This means that the extent of the ion motional state wave function is typically less than 30 nm. The lifetime of the ion motional state is relatively long, on the order of tens of milliseconds for ions trapped 40 μm from a surface in a cryogenic environment [45], and the motional state can be mapped onto long-lived electronic [46], or hyperfine, states [47]. The motional state lifetime is dominated by electric field noise of unclear origin [48]. The noise is thought to be caused by impurities adsorbed on the trap electrode surfaces and to scale as $1/d^4$ with the distance (d) of the ion from the trap electrodes [49]. The typical measured power spectral density near surfaces at cryogenic temperatures is $S_E \sim 10^{-6}\,(f/\mathrm{MHz})^{\alpha}\;(1/d/\mu\mathrm{m})^4\;(\mathrm{V/m})^2\,/\mathrm{Hz}$ [50], where α can be in the range 1–2 [51]. At room temperature, the noise is typically two or more orders of magnitude higher. Recently, the electric field noise was reduced by sputter cleaning of gold surfaces in vacuum to values comparable with those achieved in cryogenic traps [52]. However, less aggressive cleaning methods will certainly be beneficial for sensitive devices. Moreover, the effect of cleaning methods in cryogenic temperatures is unknown. This type of noise puts a limit on how close to solid-state devices trapped ions can be practically useful. As we will see in Section 6, this type of noise could severely impact the atomic systems in many hybrid device applications, and con- siderable effort is made to understand and eliminate it.

The case of mechanical oscillators, such as cantilevers, nanobeams, or membranes, is similar to that of trapped ions: The dipole is formed by the mechanical motion of electrical charge, or in the case of magnetized oscillators, of a magnetic dipole moment. Typical masses are in the pg regime, whereas the frequencies can be from a few kHz (51) to several tens of MHz (52). As a result, the extent of quantum mechanical motion, determined by the size of the ground state x0, is in the pm range. The cantilever quality factors can exceed 106 at room temperature and 10 7 at cryogenic temperature (53, 54). In the latter case,

the losses are thought to be dominated by defects acting as tunneling TLSs in the resonator material (55). Mechanical oscillators allow an interface of atomic systems with the field of cavity optomechanics, linking to a large number of systems in which quantum mechanical behavior is explored. For a recent review of these systems, see Reference 7.

The case of mechanical oscillators, such as cantilevers, nanobeams or membranes, is similar to that of trapped ions: the dipole is formed by the mechanical motion of electrical charge, or in the case of magnetized oscillators, of a magnetic dipole moment. Typical masses are in the pg regime, whereas the frequencies can be from a few kHz [53] to several tens of MHz [54]. As a result, the extent of quantum mechanical motion, determined by the size of the ground state x_0, is in the pm range. Their quality factors can exceed 10^6 at room temperature, and 10^7 at cryogenic temperature [55, 56]. In the latter case, the losses are thought to be dominated by defects acting as tunneling two level systems in the resonator material [57]. Mechanical oscillators allow an interface with the field of cavity optomechanics, linking to a large number of systems in which quantum mechanical behavior is explored. For a recent review of these systems, see [9].

Despite their large mass, and correspondingly small oscillation amplitudes, macroscopic oscillators can carry several thousand elementary charges, which makes for a dipole moment $\mu_{\mathrm{el}} = q\, x_0$ in the several Debye range. Mechanical oscillators can also carry magnetic particles. Assuming a magnetic moment $\mu \approx 10^6\, \mu_{\mathrm{B}}$, the oscillating magnet produces and oscillating magnetic field, which can mediate the coupling of the mechanical motion to other magnetic dipoles (see, for example [53, 58, 59]). The strength of the interaction with a magnetic dipole is determined by the amplitude of the oscillating magnetic field at the mechanical oscillator frequency $B = \frac{3\,\mu_0 \mu\, x_0}{2\,\pi\, d^4}$, at a distance d from the magnet. This can be viewed as arising from a magnetic dipole of the magnetized oscillator, given by $\mu_{\mathrm{mag}} = 3\,\mu\, x_0/d$, which can be several tens of Bohr magnetons.

These systems offer a large toolbox to accommodate a variety of new ideas. Out of the various solid-state and atomic systems which we will not cover in detail, we mention NV centers in diamond, which are suitable for coupling. e.g. to superconducting flux qubits [60–62]. In a way, NV centers in diamond resemble atoms trapped in a solid state diamond matrix, and show rather promising coherence times of up to seconds, if care is taken to reduce nuclear spin coupling in the diamond host [63].

Electric and magnetic dipole systems currently pursued by different experimental groups

Electric dipoles				
System	$\mu_{\rm el}$	$\omega/2\pi$	T_1	T_2
Superconducting charge qubit	10^4-10^6 D [7, 18]	1-10 GHz [19]	0.2 ms [21]	92 μs [8]
Rydberg atom	$10^3 - 10^4$ D [38]	5-50 GHz	50 μs - 1 ms [38]	(Sec. VI)
Trapped ion motion	$5 \times 10^2 - 10^3$ D [44]	0.1-10 MHz [44]	$\sim$10 ms[45]	-
Polar molecule	$1 - 10$ D [41]	1-10 GHz [42]	μs-ms (Sec. VI)	ms (Sec. VI)
Charged mechanical oscillator	2-20 D	1-50 MHz	160 ms [56]	-
Magnetic dipoles				
System	$\mu_{\rm mag}$	$\omega/2\pi$	T_1	T_2
Superconducting flux qubit	$5 \times 10^5\,\mu_{\rm B}$ [25]	1-10 GHz [19]	12 μs [64]	23 μs [64]
Magnetized mechanical oscillator	$10 - 50\,\mu_{\rm B}$ [53–55]	1-50 MHz	160 ms [56]	-
NV spin in diamond	$\sim \mu_{\rm B}$	GHz	380 s []	1.8 ms [63]
Resonators				
System	Z	$\omega/2\pi$	T_1	T_2
Lumped element resonator	$O(50)\,\Omega$	GHz	1 μs [65]	-
CPW resonator	$O(50)\,\Omega$	GHz	45 μs [35]	-

TABLE I. List of candidate systems used as electric or magnetic dipoles and resonant circuits for coupling. Typical dipole moments and transition frequencies are included. Systems are shown in order of decreasing dipole strength. The frequency ranges are indicative of typical transition frequencies, but values outside the given ranges are possible.

and their typical strengths are summarized in Table I. We now turn to the important question of how these building blocks interact with each other, and how to interconnect them.

III. DIFFERENT BUSES

As we already mentioned in the introduction, the exchange of information between different qubits can be accomplished via direct coupling, or via a mediator systems which we termed the "bus". We now discuss these possibilities in more detail.

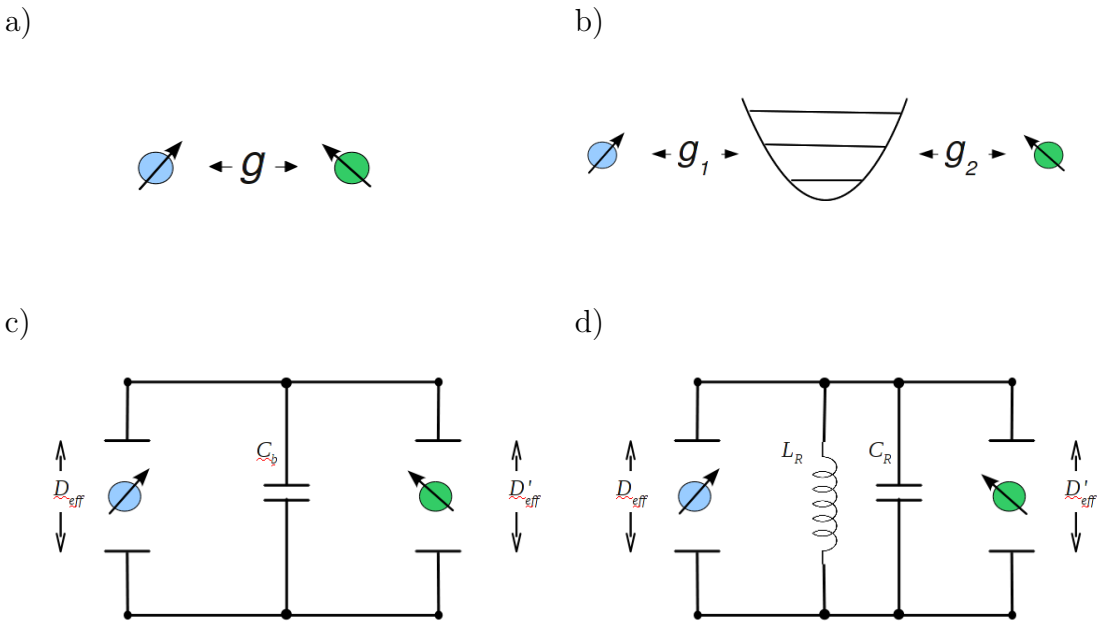

FIG. 3. (a) Qubits interconnected via electromagnetic interaction in free space (b) Harmonic oscillator bus between electrical dipoles (c) A capacitive electrostatic bus between electrical dipoles (d) A resonant electrical circuit bus.

A. Free Space Coupling

The simplest way in which two physically distinct qubits can be interconnected is by bringing them close to each other and allowing them to interact through free space, see Fig. 3a. The quantum dipole-dipole interaction, for dipoles μ_1 and μ_2, separated by $\vec{r}$, can be derived from the classical expression $U = \vec{\mu_1} \cdot \vec{\mu_2}/r^3 - 3(\vec{\mu_1} \cdot r)(\vec{\mu_2} \cdot r)/r^5$, by expressing the dipoles in terms of Pauli spin operators [66]. If the dipole quantization axis, defined by an externally applied field, is along $\vec{r}$, then this expression is of the form $\sigma_+^{(1)}\sigma_-^{(2)} + \sigma_-^{(1)}\sigma_+^{(2)} - 2\sigma_z^{(1)}\sigma_z^{(2)}$, where $\sigma_{\pm,z}^{(1,2)}$ are the usual Pauli operators. This is applicable to particles carrying spin, but not to the interaction between many of the systems mentioned in Sec. II. For example, the electrostatic interaction between two charged harmonic oscillators is of the form $a_1^\dagger a_2 + a_1 a_2^\dagger$ [45, 67], the interaction between atoms in the dipole approximation is $\sigma_+^{(1)}\sigma_-^{(2)} + \sigma_-^{(1)}\sigma_+^{(2)}$ [68], in a charge qubit the effective electric dipole is geometrically constrained along one particular direction, and likewise for the magnetic moment in a flux

qubit. Thus, in these cases the interaction can be written as

$$H = \hbar\, g\, \left(\sigma_+^{(1)}\, \sigma_-^{(2)} + \sigma_-^{(1)}\, \sigma_+^{(2)}\right) \tag{1}$$

where g is the coupling strength. The interpretation of this interaction is straightforward in the sense that it describes processes where the energy of the excitation taken out one system via the operator $\sigma_-^{(i)}$ is injected into the other system via $\sigma_+^{(j)}$.

A rather convenient way to initiate and terminate information transfer between the two qubits is usually by tuning their frequencies, ω_1, ω_2 into and out of resonance. The duration of a swap operation in this case is $\tau_{\rm swap} = \pi/g$. To generate entanglement between both qubits, we may initialize them in the state $|1\rangle|0\rangle$ and let the coupling act for $\tau_{\rm swap}/2$ generating a Bell state of the form $(|0\rangle|1\rangle + |1\rangle|0\rangle)/\sqrt{2}$ [69].

Free-space coupling has the advantage of simplicity, but, as we discussed in the previous section, it requires that the different qubits be brought in close proximity to each other. This is not always feasible and can pose limitations to the scalability of the hybrid device. Usually stronger and more easily scalable coupling can be obtained by allowing the qubits to interact through an engineered bus.

B. Harmonic Oscillator

The bus is in many cases a harmonic oscillator, as shown on Fig. 3b,d. Here we represent the bus oscillator as a lumped element circuit, but it can be a standing wave in a cavity [18], or even a mode of a small size mechanical oscillator. The dipole-field interaction is $-E\,\mu_{\rm el}$ for electric dipoles and $-B\,\mu_{\rm mg}$ for magnetic dipoles. If the dipoles are expressed in terms of Pauli operators, and the voltage and current of the oscillator in terms of creation and annihilation operators, these interactions take the form

$$H = \hbar\, g_1\, \left(\sigma_+^{(1)}\, a_{\rm bus} + \sigma_-^{(1)}\, a_{\rm bus}^\dagger\right) + \hbar\, g_2\, \left(\sigma_+^{(2)}\, a_{\rm bus} + \sigma_-^{(2)}\, a_{\rm bus}^\dagger\right) \tag{2}$$

where the coupling strengths g_1, g_2 are determined by the treatment leading to Eqs. 13,14. The bus can can be detuned from the qubit resonance frequency by $\Delta = \omega_{\rm bus} - \omega_1$ ($\omega_1 = \omega_2$). This offers one more tunable element in the device, which comes with added flexibility but also higher complexity and potentially additional sources of noise.

In some cases, the qubits can be very strongly coupled to the oscillator. This allows operation of the bus in the dispersive regime, $\Delta \gg g$, where the detuning between qubits and oscillator is far larger than the coupling rate. The main advantage here, is that the resonator mode is only weakly populated while information is transferred through the bus, thus reducing the sensitivity of the hybrid system to decoherence in the bus. Nevertheless, strong coupling is not always feasible, or it can come at the expense of increased decoherence on the qubits themselves (see Sec. V), and operation of the bus in the regime of small or zero detuning can be preferable.

For resonant coupling and $g_1 = g_2 = g$, the time for a swap operation is $\pi/\sqrt{2}g$, while for dispersive coupling $\tau_{\rm swap} = \pi\Delta/2g^2$ and $\tau_{\rm Bell} = \tau_{\rm swap}/2$. In general, in the resonant case there exists no point in time at which the two qubits are in a Bell state, since some population is always found in the bus. This can be solved by choosing 'magic' detunings, for which the population in the bus vanishes when the qubits are in a Bell state [70, 71]. In general the same is true of the dispersive system as well, but in this case the probability amplitude in the bus is only of order g/Δ (i.e. the population is g^2/Δ^2). Thus, in principle a dispersive bus can produce Bell states and full population exchange to arbitrary fidelity, for arbitrary detuning.

C. Far Off-Resonant Oscillator

There is one more form of bus which is worth mentioning due to its wide applicability, the far-dispersive capacitive bus, see Fig. 3c. This type of bus has been proposed for interconnecting electrons trapped in Penning traps to ions [15], Rydberg atoms to each other [39], trapped ions to superconducting charge qubits [72], electrons trapped in Penning traps to each other [73, 74], trapped ions in Paul traps to each other [75] and charged nanobeams [76]. The capacitive bus falls in-between the two categories mentioned above. It can be viewed as a far off-resonant limit of the harmonic oscillator bus. But it can also be viewed as a modification of the electrostatic free-space bus in which the boundary conditions of free space have been modified to optimize the coupling strength. It provides a convenient solution for situations in which a resonant oscillator bus cannot be used, for example if the coupling rate of the dipoles to the bus cannot be made much stronger than the decoherence rate of the bus itself (i.e. if the so-called "strong coupling" regime cannot be reached). In

practice, the latter means that at frequencies below the GHz range a capacitive bus might be the best option, since the thermal population in the bus will be rather high, even at dilution refrigerator temperatures.

D. Parametric Frequency Conversion

In many situations, the different qubits are not resonant with each other, or with the bus, and are not sufficiently tunable to achieve fast and switchable quantum state transfer between the two. In these situations, a tunable coupling element offers the solution of coupling via parametric frequency conversion between the different quantum stages [77]. During this process, the non-linear coupling element is classically driven at the difference frequency $\delta\omega = \omega_1 - \omega_2$ between the two non-resonant quantum modes, giving rise to parametric coupling which oscillates at the difference frequency $g(t) = g_0 \cos(\delta\omega\, t)$. This effect is more clear in the interaction picture. We consider two non-resonant oscillators, coupled with a time dependent strength

$$H = \hbar\omega_1 a_1^\dagger a_1 + \hbar\omega_2 a_2^\dagger a_2 + \hbar\, g_0 \cos(\delta\omega\, t)\, \left(a_1^\dagger a_2 + a_1 a_2^\dagger\right) . \tag{3}$$

In the interaction picture, this Hamiltonian can be shown to be [78]

$$H = \hbar\, g_0 \cos(\delta\omega\, t)\, \left(e^{i(\omega_1-\omega_2)t} a_1^\dagger a_2 + e^{-i(\omega_1-\omega_2)t} a_1 a_2^\dagger\right) . \tag{4}$$

In the rotating wave approximation, the interaction term survives under the resonance condition $\delta\omega = \omega_1 - \omega_2$, and population exchange between the two oscillators occurs at a rate $g_0/2$, The factor $1/2$ can be understood classically as the result of creating two equal sidebands on the first oscillator, of which only one couples to the second one. The above can also be seen by solving the Heisenberg equations of motion for the parametrically driven system in the rotating wave approximation [77]. Parametric frequency conversion results in full state exchange between two off-resonant systems with, in principle, no added noise. It can be viewed as a process in which a classical drive field contributes or absorbs photons at the energy difference $\hbar\,\delta\omega$ between the two modes, so that energy conservation is satisfied during the state transfer.

IV. SUMMARY OF INTERACTIONS

In most applications of atomic physics, the experimental control parameters for the atomic systems are electromagnetic. Thus, it is not surprising that in hybrid devices where one component is an atomic system, the interactions between the different components are of electromagnetic nature. These can be electric or magnetic, depending on whether the quantum systems in question carry electric charge, electric dipole moment, or magnetic dipole moment. In the most general cases, it can be instructive -or even necessary- to obtain the strength of the interaction between the quantum systems by integrating the electromagnetic energy density over an appropriate volume of the device. Nevertheless, in most cases, the quantum systems can be viewed as elementary dipoles or as electromagnetic harmonic oscillators. The interaction strengths are then given by the usual expressions for dipole-dipole and dipole-field interactions. In what follows, we review the basic interactions that one is likely to encounter in hybrid devices. We try to emphasize a common treatment between different systems, as well as the differences between them. We show that typical electric coupling strengths are significantly stronger than magnetic coupling strengths. We also summarize the coupling of elementary dipoles to resonators and emphasize the role of characteristic impedance on the coupling rates.

A. Interaction Strength and Characteristic Impedance

The coupling rate between different systems depends on the strength of the interaction and on the characteristic impedances of the systems. Characteristic impedance turns out to be a useful concept in hybrid system considerations. Classically, the characteristic impedance of a harmonic oscillator describes how fast its energy responds to an external driving force of a given amplitude. It also describes the relative magnitude of the values of the conjugate variables for a given energy in the system. Quantum mechanically, the characteristic impedance determines the relative magnitude of quantum fluctuations of the conjugate variables. For example, a large impedance LC resonator has large voltage fluctuations and small current fluctuations. It is instructive to see this both classically and quantum mechanically in a simple coupled mechanical oscillator model. The example can easily be translated to other systems, such as electrical circuits.

1. Classical coupled oscillators

To see this, consider two harmonic oscillators, with masses m_1 and m_2, each one in a harmonic potential with frequency ω. The interaction strength between the oscillators is κ, i.e. for displacements x_1, x_2 from equilibrium, the interaction energy is $U = \kappa\, x_1\, x_2$. The characteristic (mechanical) impedance, Z_i, $i = 1, 2$, for each oscillator determines the relative magnitude of the conjugate variable oscillations $Z_i = p_{i,\max}/x_{i,\max} = m_i\,\omega$. Now, if a certain amount of energy is stored in each of the two oscillators, their respective oscillation amplitudes are related by $\frac{x_{1,\max}}{x_{2,\max}} = \sqrt{\frac{Z_2}{Z_1}} = \sqrt{\frac{m_2}{m_1}}$., i.e. the impedance mismatch determines the relative scale of amplitudes corresponding to the same amount of energy.

It follows from the form of the interaction energy, that the force on the second oscillator when the first is displaced by x_1 is $-\kappa\, x_1$. Consequently, if all the energy of the system is stored momentarily in the first oscillator and it oscillates with $x_{1,\max}$, the second oscillator is being driven by a force of amplitude $f_{2,1} = \kappa\, x_{1,\max} = \kappa\sqrt{\frac{Z_2}{Z_1}}\, x_{2,\max}$, where in the second step we expressed the force in terms of the maximal amplitude, $x_{2,\max}$, of the second oscillator.

When it is driven by this force, the oscillation amplitude of the second oscillator will grow at a rate $\frac{f_{2,1}}{2Z_2} = \frac{\kappa}{2\,m_2\,\omega}\sqrt{\frac{Z_2}{Z_1}}\, x_{2,\max}$. Since $x_{2,\max}$ is the amplitude of the second oscillator when all the initial energy has been transferred it, the coupling rate will be, up to numerical factors,

$$\frac{\kappa}{2\,m_2\,\omega}\sqrt{\frac{Z_2}{Z_1}}\,. \tag{5}$$

The interpretation of this process is quite simple: the strength of the interaction, and the characteristic impedance Z_2, set a natural time scale $\frac{\kappa}{2\,Z_2}$ for how long it takes to transfer energy to the second oscillator. The ratio of characteristic impedances describes the oscillation amplitude imbalance that has to be bridged for energy transfer to take place. It is straightforward to carry out a similar treatment in the case of non-mechanical oscillators.

2. Quantum coupled oscillators

To see the above results formally, the oscillator variables can be expressed in terms of second quantization operators. Then, by introducing the second quantization expressions $x_i = \sqrt{\frac{\hbar}{2\,Z_i}}\left(a_i^\dagger + a_i\right)$, the interaction term in the Hamiltonian becomes (in the rotating wave

approximation)

$$U = \frac{\hbar\kappa}{2\sqrt{Z_1 Z_2}} \left(a_1^\dagger a_2 + a_1 a_2^\dagger\right) . \tag{6}$$

The prefactor in this expression corresponds to the expression in Eq. 5, motivated by our classical discussion, but written in this form, the symmetry between the oscillator characteristic impedances is evident. The ratio $\kappa/\sqrt{Z_1 Z_2}$ describes the relative scale of the coupling interaction and the individual (uncoupled) oscillator energies.

The above example applies equally well to coupled electrical oscillators. The methods for canonical quantization of such circuits will not be covered here, the interested reader can refer to [79]. Without focusing on a particular topology, we consider two coupled LC oscillators, for which the interaction energy, expressed in canonical charge variables, q_i, $i = 1, 2$, is $U = \kappa q_1 q_2$. Then, the result in Eq. 6 holds, with the impedances Z_1, Z_2 corresponding to the characteristic impedances of the two electrical oscillators. It is instructive to contrast this example with that of two electrical oscillators coupled by an inductive term of the form $U = \lambda\Phi_1\Phi_2$, with Φ_i denoting the node flux variables [79]. Then the corresponding interaction term becomes

$$U = \frac{\hbar\lambda\sqrt{Z_1 Z_2}}{2}\,\mathrm{i}\,\left(a_1^\dagger a_2 + a_1 a_2^\dagger\right) . \tag{7}$$

We see that the characteristic impedance of the resonator plays a different role in the cases of capacitive (electric) and inductive (magnetic) coupling. We will see this again in Sec. IV D, and also in Sec. III B, where we will discuss how it determines the requirements for impedance matching of a quantum bus to different dipoles.

3. Mechanical oscillators as dipoles

We already mentioned that mechanical oscillators carrying a charge or a magnetic moment interact electromagnetically as if they carry an effective dipole moment. It is useful to adopt this view in order to put different systems on a similar footing and compare their coupling strengths to each other. Before characterizing the strength of different interactions, we discuss this equivalence.

First we consider the case of a charged oscillator, carrying charge q. When the oscillator is displaced from equilibrium by x, it interacts with electric fields as $U_{\mathrm{el}} = -q\,x\,E$. This

suggests that the electric dipole moment be $\mu = q\,x$. Quantum mechanically, the dipole operator can be written $\mu = q\sqrt{\frac{\hbar}{2\,m\,\omega}}\,\left(a^\dagger + a\right)$, where m is the mass and ω the frequency of the oscillator. The electric dipole moment of the harmonic oscillator is then

$$\mu_{\rm el} = q\sqrt{\frac{\hbar}{2\,m\,\omega}}\,. \tag{8}$$

It is straightforward to extend this treatment to magnetized oscillators, for example a nanobeam with a magentized tip [53, 59]. This situation is not completely analogous to that of a charged oscillator, because a magnetized object produces around it a dipole field, $B_{\rm osc} \sim \mu/r^3$, where μ is the dipole moment of the magnetized tip, and r the distance from the tip. The result is that an elementary dipole $\mu_{\rm B}$ a distance r away from the magnetized tip interacts with the oscillating part of the magnetic field, and the interaction is $U = \mu_{\rm B}\,\frac{\partial B}{\partial r}\,x$. From this, it is straightforward to see that quantum-mechanically, the magnetized oscillator is equivalent to a magnetic dipole of strength $\mu_{\rm eff} = \mu\,\frac{3\,x_0}{r}$, as already mentioned in section II.

We now proceed to discuss the typical interaction strengths between different systems.

B. Dipole-Dipole Interaction

As we already saw, the quantum systems considered for hybrid applications typically carry an electrical dipole moment, or a magnetic dipole moment. In some situations dipole-dipole interactions in free space can be utilized to couple such systems with each other. An important difference between the two is that typical magnetic interaction strengths are weaker than electric interaction strengths.

For magnetic dipoles, typical magnetic moments can be expressed in terms of Bohr magnetons $\mu_{\rm B}$ (see Table I). The scale of the interaction strength is

$$U_{\rm mg} = \frac{\mu_0 \mu_{\rm B}^2}{2\pi r^3}\,. \tag{9}$$

At a distance of 1 μm, this is a weak $2\pi\times$26 mHz.

For electrical dipoles, the coupling is stronger. Typical dipole moments can be expressed

in units of Debye. The interaction strength is

$$U_{\rm el} = \frac{\mu_{\rm el}^2}{2\pi\epsilon_0 r^3}\,, \tag{10}$$

and we choose $\mu_{\rm el} = e\,a_0/2$, which is close to 1 D. At a distance of 1 μm, the interaction strength is $2\pi\times488$ Hz.

It is interesting, but not surprising, that for the above choice of typical dipole strengths:

$$\frac{U_{\rm mg}}{U_{\rm el}} = \alpha^2\,, \tag{11}$$

where α is the fine structure constant. Here, it is important to appreciate that the weakness of magnetic interactions is not necessarily a disadvantage of magnetic dipole systems. The reduced coupling strength comes with the potential advantage of higher immunity to environmental decoherence. In fact, elementary magnetic dipoles, such as nuclear spins in diamond-NV centers, can offer the longest lived solid-state qubit candidates, provided that the dominant decoherence mechanisms are electromagnetic in nature, and that the nuclear spin environment is sufficiently well controlled [63].

C. Electrical Dipole Capacitive Bus

The coupling strength between two electrical dipoles can be increased over the coupling strength achieved in free space by placing a coupling electrode between them [15, 39, 73, 75]. This electrode acts as the quantum bus connecting the two dipoles. More specifically, each dipole induces image charges in the coupling wire and, in this way, interacts electrostatically with the other dipole. The image charges are distributed over the length of the wire and as a result the strength of the interaction is inversely proportional to the capacitance of the coupling electrode to ground. This system is well described by the circuit shown in Fig. 3c). The interaction strength is given by

$$U_{\rm el} = \frac{\mu_{\rm el}^2}{D_{\rm eff}^2 C} \tag{12}$$

where for simplicity we have chosen the same dipole moments, $\mu_{\rm el}$, and effective distances, $D_{\rm eff}$, on both sides of the bus. The effective distance $D_{\rm eff}$ is related to the physical distance

between the electrodes which pick up the electrical signal by a geometric factor of order unity [80, 81]. C is the parasitic capacitance of the bus to ground.

The capacitive bus in effect shortens the distance between the electrical dipoles leading to $1/r$ instead of the $1/r^3$ scaling of free-space coupling. In many situations [75], the parasitic capacitance can be made as small as a few fF for length of a few hundred micrometers. A typical coupling strength at effective distance $D_{\rm eff} = 1\,\mu$m, $\mu_{\rm el} = e\,a_0/2$, and $C = 1$ fF is $2\pi\times 27$ Hz. The capacitive bus offers an enhancement to free-space coupling, but if the qubit frequencies are high enough that a resonator can be used to transfer information (see Sec. III B), the latter can provide higher coupling rates and increased protection against noise. We now look at the interaction strengths obtained in this case.

D. Dipole-Resonator Interaction

A rather fruitful approach is to couple an electric or magnetic dipole to an electromagnetic oscillator, which plays the role of a bus between distant dipoles, as in the example of superconducting cQED [18]. This approach offers a combination of high coupling strength and filtering of unwanted noise, with the potential of scalability to large numbers of devices.

We now discuss how individual dipoles couple to a resonator. The magnitudes of quantum zero point voltage and current fluctuations in the oscillator satisfy $Z = V_0/I_0$, where Z is The characteristic impedance of the oscillator. Voltage fluctuations can couple to electrical dipoles via an electric field, and current fluctuations, can couple to magnetic dipoles via a magnetic field, and the characteristic impedance determines the magnitude of these coupling strengths.

To obtain the interaction of electrical oscillators with elementary dipoles, we consider an oscillator which is either producing an electric field $E = V/D_{\rm eff}$ between the electrodes of some capacitive configuration, or a magnetic field $B = \mu_0\, I/D'_{\rm eff}$ near some inductive configuration. Here $D_{\rm eff}$ and $D'_{\rm eff}$ are effective dimensions of the electrode structures producing the coupling fields. The electrical oscillator can be a lumped element circuit, or a standing-wave transmission line resonator, with the transmission line impedance Z.

The interaction strength for an electric dipole is $\mu_{\rm el}E_0$, which gives

$$U_{\rm el} = \frac{V_0\mu_{\rm el}}{D_{\rm eff}} = \frac{\omega\,\mu_{\rm el}}{D_{\rm eff}}\sqrt{\frac{\hbar\,Z}{2}}\,, \tag{13}$$

where ω is the oscillator frequency and V_0 describes the amplitude of quantum voltage fluctuations. Likewise, for a magnetic dipole the strength is $\mu_{\rm mg} B_0$, or

$$U_{\rm mg} = B_0 \mu_{\rm mg} = \frac{\omega\, \mu_{\rm mg}}{D'_{\rm eff}} \sqrt{\frac{\hbar}{2\, Z}}\,. \tag{14}$$

The interaction strength is proportional to the resonator frequency, due to the scaling of zero point current and voltage fluctuations with frequency.

It is straightforward to see that for the choice of dipoles used in the previous section, the strengths of the electric and magnetic coupling satisfy

$$\frac{U_{\rm mg}}{U_{\rm el}} = \alpha\, \frac{Z_0}{Z} \frac{D_{\rm eff}}{D'_{\rm eff}} \tag{15}$$

where $Z_0 \approx 377\,\Omega$ is the impedance of free space. So we see that the optimal parameters of an oscillator bus are determined by the type of dipole one couples to: electric dipoles are favored by large impedances, whereas magnetic dipoles by small impedances. The coupling between an oscillator and a magnetic dipole will gain from small impedances as $1/\sqrt{Z}$, while electric coupling will gain from large impedances as $\sqrt{Z}$. To get a feeling for typical values, at effective distances of 1 μm, impedance of $50\,\Omega$, frequency $2\pi\times5$ GHz, the coupling strength is $2\pi\times20$ kHz for an electric dipole of $e\, a_0/2$, and $2\pi\times560$ Hz for a magnetic dipole of $\mu_{\rm B}$.

It is useful to also summarize the equivalent results for transmission line resonators. A finite length of an appropriately terminated transmission line forms a one-dimensional electromagnetic cavity, and can act as an electrical resonator. In this case, the quantum fluctuations of voltage get reduced as $1/\sqrt{l}$, with the length, l, of the resonator [82]. A $\lambda/4$ transmission line, the other side of which is shorted, behaves as a lumped-element LC resonator with characteristic impedance $4Z/\pi$, where Z is the transmission line characteristic impedance. In general, the open end of a length $n\lambda/4$, $n = 1, 2, ...$ of transmission line with impedance Z, of which the far end is shorted (n odd) or an open circuit (n even), behaves as an LC resonator with characteristic impedance $4Z/(n\pi)$ [83].

The above properties of the harmonic oscillator bus, offer guidelines as to what the optimal impedance is. So long as one stays within the electrical dipole or magnetic dipole approximation, then electrical dipoles couple stronger the higher the characteristic impedance

is, and inversely magnetic dipoles benefit from small impedances. However, in the case where a bus is used to mediate the coupling of an electric dipole to a magnetic dipole, see Sec. III B, there exists an optimal impedance at which the coupling rate of the bus to each of the two dipoles is the same. If the oscillator impedance deviates from this value, there will be no condition under which full population transfer can be achieved between the dipoles, unless the bus is used dispersively. From Eq. 15, we see that the optimal bus impedance is $Z_{\rm opt} = \alpha Z_0 \frac{D_{\rm eff}\mu_{\rm el}}{D'_{\rm eff}\mu_{\rm mg}}$, where as we mentioned before, $D_{\rm eff}$ and $D'_{\rm eff}$ are effective distances for the electrodes that couple to the dipoles. [84]. This feature of the harmonic oscillator bus is, in a way, a generalized form of impedance matching requirement, and it is related to the fact that impedance is a measure of the values of the conjugate variables in a harmonic oscillator.

E. Trapped Ion and Mechanical Oscillator

In light of developments in merging nanomechanics with other technologies [54, 85], coupling of atomic systems to mechanical oscillators could become promising, e.g. if the mechanical system acts as a transducer from the ion motion to electrical signals. We discuss now a trapped ion (or a small ion string) coupled to a charged nanobeam. We assume that the ion is trapped a distance d from the beam and interacts via the Coulomb interaction energy. One might reason that the coupling can be boosted to arbitrary values by increasing the charge Q on the nanobeam. However, if we continue to charge the nanobeam, the ion resonance frequency will increase. In the limit that all the restoring force on the ion comes from the charge of the nanobeam, the ion frequency is given by the curvature of the electrostatic potential of the oscillator at the ion position $\frac{1}{2\pi\epsilon_0}\frac{eQ}{d^3}$. Inserting this equality in Eq. 6 and assuming resonance, i.e. $\omega_{\rm b} = \omega_{\rm i}$, we find that for the coupling constant g

$$g = \frac{\omega}{2}\sqrt{\frac{m_{\rm i}}{m_{\rm b}}}\,, \tag{16}$$

where $m_{\rm i}$ and $m_{\rm b}$ refer to the ion and nanobeam mass, respectively. Referring back to our discussion at the beginning of this section, this corresponds to setting $\kappa = m\,\omega^2$ in Eq. 6. For a typical mass of a nanobeam of 0.1 pg, using a heavy ion, such as $^{199}Hg^+$ and a large frequency $\omega = 2\pi \times 10$ MHz, we arrive a coupling on the order of $2\pi \times 20$ Hz. We will later

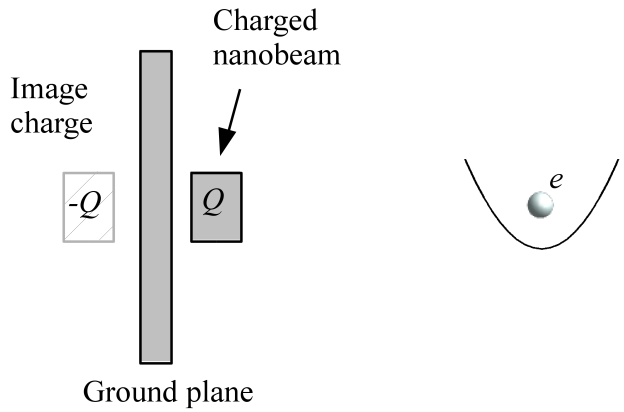

FIG. 4. A trapped ion (right) with charge e interacting with a charged nanobeam with charge Q and its image charge $-Q$ induced in a ground plane.

discuss two proposals in this direction.

In Eq. 16 we assumed that both the coupling as well as the confinement of the ion come from the charge on the nanobeam. We call the coupling deduced under this condition the natural coupling which can be only overcome by introducing an anti-confining potential for the ion. An experimentally attractive way to induce anti-confinement is by using image charges induced in an electrode near the nanobeam (see Fig. 4). Such an electrode placed behind the nanobeam acts as an additional ground plane and the negative image charge nearly compensates the force of the beam on the ion, while at the same time doubling the coupling.

The interaction energy is now $U = \frac{eQ}{4\pi\epsilon_0}\left(\frac{1}{|d-x_\mathrm{i}-x_\mathrm{b}|} - \frac{1}{|d-x_\mathrm{i}-x_\mathrm{b'}|}\right)$. Here x_i and x_b are the displacements of the ion and the nanobeam from their respective equilibrium positions, and $x_{b'} = -x_b$ is the displacement of the image charge, $-Q$. For displacements x_i, x_b, much smaller than the distance, d, of the ion to the beam, this can be expanded to give an interaction term $U = -\frac{e}{4\pi\epsilon_0}\left(\frac{Q}{d^3}x_\mathrm{i}x_\mathrm{b} + \frac{(-Q)}{d^3}x_\mathrm{i}x_\mathrm{b'}\right)$. Using $x_\mathrm{b'} = -x_\mathrm{b}$, we see that the interaction of the ion with the nanobeam, $\frac{\partial U}{\partial x_\mathrm{b}}$, doubles while the influence of the interaction potential on the ion confining potential (the trapping potential), $\frac{\partial^2 U}{\partial x_\mathrm{i}^2}$, cancels. Thus, the coupling can be increased up to the point where one of the assumptions fails, for instance, when nanobeam is pulled so strongly towards the ground plane that it sticks to it or when the force on the ion is not fully canceled [86].

V. DECOHERENCE

To assess the usefulness of a hybrid device, one needs to understand what the constituent qubits couple to, and how strongly. The main challenge lies in maximizing the coupling between the qubits, while maintaining minimal coupling to unwanted environmental degrees of freedom.

This can be a demanding task, since very often the close proximity of physically different qubits to each other or to a bus causes additional decoherence. For example, an electrical dipole brought close to a metal surface will experience increased electric field noise of the type encountered in ion trap experiments [49], and the noise is likely to be also present near non-metallic surfaces [87]. This type of noise will change the energy of the dipole at a rate $\gamma_1 = \frac{S_E(\omega)\mu_{\rm el}^2}{2\hbar^2}$, where $S_E(\omega)$ is the electric field noise spectral density at the dipole transition frequency.

A second type of decoherence occurs if the energy splitting of the dipole states depend on static fields, for example through a static Stark shift. For example, for a system with a linear Stark shift with strength $\frac{\partial\omega}{\partial E}$, the presence of $1/f$ electric field noise described by $S_E = E_0^2/f$, causes dephasing at a rate $\gamma_\varphi \approx \frac{\partial\omega}{\partial E}E_0$. For a quadratic Stark shift, the dephasing rate is $\gamma_\varphi \approx \frac{\partial^2\omega}{\partial E^2}E_0^2$. Effects like this need to be considered in the design and implementation stage of hybrid quantum systems. As we will discuss in the next section, all possible hybrid quantum systems face limitations and challenges related to environmentally caused decoherence.

The first of the decoherence processes in the above example, causes energy exchange between the quantum system and the enviroment, i.e. dissipation and heating, and is often summarized as energy relaxation and referred to as a T_1 process. In the second example there is no energy exchange, but the phase evolution of superpositions of energy eigenstates depends on the enviroment, and consequently the phase information of the superposition is lost. This latter process is often referred to as pure dephasing, or a T_φ process. Note that a pure energy relaxation mechanism will by itself cause dephasing at rate $\frac{1}{2T_1}$, so that the total, or effective, dephasing time constant, T_2, measured in experiments will be the sum of the pure phase damping and the phase damping caused by the energy relaxation processes:

$$\frac{1}{T_2} = \frac{1}{2T_1} + \frac{1}{T_\varphi}\,. \tag{17}$$

.

The effect of a dissipative environment on a quantum system is described very well in the master equation formalism, where the time evolution of the density matrix acquires non-unitary components. We adopt this description here. We model the enviroment as a bosonic bath with mean thermal energy kT, and some additional dephasing mechanisms . The quantum system interacts with a modes b of the bath via an interaction of the form $\kappa(a^\dagger b + a b^\dagger)$ which describes energy relaxation. A pure dephasing process can be described mathematically as a projection of the system onto the energy eigebasis. Such an energy measurement can be modeled by the interaction term $\kappa' a^\dagger a \left(b' + b'^\dagger\right)$ where the environment mode, b', is modeled, for instance, as a single oscillator acting as a measurement device. Note that in the context of quantum information, decoherence is meaningfully applied to individual quantum systems by taking the average over many repetitions of particular realizations of the quantum dynamics. Using this approach, we can introduce a density matrix formalism for individual quantum systems and arrive at the following equations of motion for the reduced density matrix (i.e. after the environmental degrees of freedom have been traced out) [78, 88]:

$$\begin{aligned}\partial_t \rho = & -\frac{i}{\hbar}\,[\rho,\, H] \\ & + \frac{\gamma}{2}(\bar{n}+1)(2a\rho a^\dagger - a^\dagger a\rho - \rho a^\dagger a) + \frac{\gamma}{2}\bar{n}(2a^\dagger \rho a - a a^\dagger \rho - \rho a a^\dagger) \\ & + \frac{\gamma_\varphi}{2}(2a^\dagger a \rho a^\dagger a - a^\dagger a a^\dagger a \rho - \rho a^\dagger a a^\dagger a)\,. \end{aligned} \tag{18}$$

The first term describes the coherent evolution of the density matrix, fully equivalent to the Schrödinger equation, the second line energy relaxation including the inevitable phase damping (the T_1 process) and the last term pure phase damping γ_φ with time constant T_φ.

Before getting into the specifics of different quantum systems, it is useful to discuss in qualitative terms how the different sources of dissipation affect the behavior of a hybrid system. This can be illustrated by the elementary building blocks of Fig. 3(a), 3(b). A useful measure of the effect of dissipation is the fidelity of an operation, defined as $F = tr\left(\sqrt{\rho^{1/2}\rho_{\text{ideal}}\rho^{1/2}}\right) = \sqrt{\langle \Psi_{\text{ideal}} |\rho| \Psi_{\text{ideal}}\rangle}$, where ρ and $\rho_{\text{ideal}} = |\Psi_{\text{ideal}}\rangle\langle\Psi_{\text{ideal}}|$ are the density matrices of the actual and ideal final quantum states, and $tr(A)$ is the trace of operator A [89]. We are interested in the fidelity of a swap operation in the presence of decoherence acting both on the qubits as well as on the bus. A source of decoherence with rate γ, acting

on one component of a quantum system, during some operation with duration τ, will cause loss of fidelity which is proportional to $\gamma\,\tau$, if $\gamma\,\tau \ll 1$. A decoherence source acting on one component, e.g. on one qubit, causes loss of fidelity which depends strongly on the time averaged population amplitude of that component. This implies, for example, that the infidelity of a swap operation caused by a lossy bus can be limited by using the bus off-resonantly. In the case of environmental thermal (sometimes called Brownian) noise, the effect of noise is proportional to the mean thermal occupation number of the mode, $n_{\rm th}$. Then, the infidelity is proportional to $\gamma\,\tau\,n_{\rm th}$. This illustrates one of the main advantages of operating quantum devices at mK temperatures and GHz frequencies, where thermal environmental effects cause little influence to quantum coherent device operation.

It is straightforward to numerically solve the master equation for a swap operation and extract the typical scaling of fidelities using available open quantum system simulation packages such as qutip [90]. We find that the swap fidelity decreases with the strength of decoherence, Γ, as $\frac{dF}{d(\Gamma\,\tau_{\rm swap})} = -r$, where Γ is either $n_{\rm th}\gamma$ or γ_φ. By looking at states of the form $a\,|000\rangle + b\,|100\rangle$, where the tensor products are understood to refer to $|{\rm qubit}_1\rangle \otimes |{\rm bus}\rangle \otimes |{\rm qubit}_2\rangle$, we find a value of r which varies between 0.2 and 0.5 depending on the source of dissipation, and the quantum state being swapped. For example pure dephasing will influence the state $\frac{1}{\sqrt{2}}\,(|000\rangle + |100\rangle)$ stronger than it will influence the state $|100\rangle$.

VI. SPECIFIC DIRECTIONS IN QUANTUM HYBRID SYSTEMS

Here we look at specific experimental proposals. We cover schemes proposed to couple trapped ions to radio-frequency electrical circuits [15], trapped ions to microwave circuits [16], trapped ions to charge qubits [72], Rydberg atoms to each other via superconducting microwave electrical circuits [39], polar molecules to superconducting microwave circuits [42, 43], and trapped ions to mechanical oscillators [91, 92].

The idea of coupling individual atoms, or electrons, to solid-state devices is significantly older than modern, quantum-information inspired hybrid devices. Single electrons (or ions) in Penning traps, coupled to lumped-element electrical resonators have formed the basis for a long series of high-precision measurements [93]. In these experiments, the role of the resonator has been to cool the trapped particle to the temperature of a cryogenic heat bath, and to perform impedance matching between the high characteristic impedance element on

the trapped-particle side, and a low characteristic impedance solid-state amplifier [94]. The successful application of laser cooling techniques to atomic systems caused a significant shift in the way this basic system was viewed. It was realized that the roles of a trapped ion and an electrical circuit could be reversed, allowing the trapped ion to act as a "refrigerator" for the resonant circuit, as well as an increased sensitivity readout device [15]. In the modern context of quantum information science, a variety of specific ideas for quantum hybrid devices have emerged. We now discuss specific proposals in this direction.

A. Trapped Ions and LC Resonators

The idea here is to couple the motion of a trapped ion to an electrical resonator, and to use the ion to laser cool the oscillator [15]. Although this experiment does not hold the prospect of becoming a useful as a hybrid quantum platform, it has the advantage that it can be realized with already established technology.

The experiments can be realized with single ions or small ion crystals trapped in a harmonic RF-trap. The leads of a tank circuit are attached to two trap electdodes and couple the circuit to the ion motion (see Fig. 5). The coupling rate follows from Eqs. 8,13, and can be seen to be $g = \frac{\omega}{2}\sqrt{\frac{e^2 L}{m D_{\rm eff}^2}} = \frac{\omega}{2}\sqrt{\frac{Z}{Z_{\rm ion}}}$, where L is the inductance of the resonator, Z the resonator characteristic impedance, $L_{\rm ion} = \frac{m D_{\rm eff}^2}{e^2}$ is the kinetic inductance of the ion and $Z_{\rm ion}$ the characteristic impedance corresponding to the ion equivalent circuit in this setting [15], m is the mass of the ion, $D_{\rm eff}$ the effective distance for the electrodes to which the ion motion couples, and ω the frequency of the ion and the resonator [95]. For an effective distance $D_{\rm eff} = 50\,\mu$m, inductance $L = 10$ mH, capacitance $C \approx 2.5$ pF, and a single $^{40}Ca^{+}$ion with a trap frequency of $2\pi \times 1$ MHz, the coupling strength is $g \approx 2\pi \times 600$ Hz. We note that for these settings, $L_{\rm ion} \approx 6.5\,$kH, and $Z_{\rm ion} \approx 41\,$GΩ. If ion strings of N ions are used, the coupling rate to the center of mass mode increases as $\sqrt{N}$, and for 10 ions the coupling rate can be increased to approximately $2\pi \times 2.0$ kHz.

To operate in the strong coupling regime, the damping constant γ of the tank circuit needs to be smaller than g. At frequencies in the MHz range, quality factors approaching 50,000, corresponding to $\gamma \approx 126\,{\rm s}^{-1}$, have been reported for superconducting coils [96], and the strong coupling regime is within reach. In the strong coupling regime, we expect that the resonant mode of the tank circuit can be cooled significantly if brought into resonance

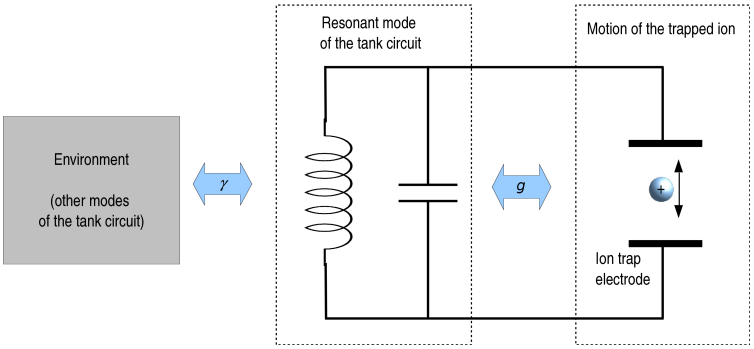

FIG. 5. Schematics of a tank circuit (center) coupled to a trapped ion (right) and the enviroment (left).

with ultra-cold ions. For the parameters of a 10 ion string given above and using $T_{\rm env} = 4$ K, the resonant mode of the tank circuit can be cooled to 63 mK, a factor of more than 60 below ambient.

Lastly, we estimate the prospects of entangling the ion motion with the superconducting circuit. The main impediment towards this goal, is that the mean occupation number of the LC oscillator in thermal equilibrium with the 4 K bath, is on the order of $kT_{\rm env}/\hbar\omega \approx 80\,000$. Therefore, the resonant circuit picks up one quantum every $\hbar\omega/\gamma_{\rm env}kT_{\rm env} \approx 0.2$ μs despite its high quality factor. By increasing the trap frequency to 10 MHz, and moving the ion closer to the pick-up electrodes to achieve an effective distance of 25 μm, the coupling rate can be increased to $g \approx 2\pi \times 39.8$ kHz for 10 ions. Additionally lowering the ambient temperature to 50 mK, and working with a quality factor on the order of 3×10^5 would be sufficient to allow cooling of the resonant mode of the tank circuit to a mean occupation number of $\frac{n_{\rm th}\gamma\pi}{2g}$ $\approx$0.14 photons. If the resonator mode is cooled to this low occupation number, the resonator and a second 10 ion string can subsequently be prepared in a Bell state $\frac{1}{\sqrt{2}}(|0\rangle|1\rangle + |1\rangle|0\rangle)$ with fidelity of 90%.

B. Coupling Ions via Parametric Frequency Conversion

The range of motional frequencies of trapped ions can be insufficient for coupling to a wide variety of electrical oscillators, for instance to microwave resonators, but parametric frequency conversion schemes can remove this limitation, as discussed in [15, 16]. Here, we outline the details of the latter of these two proposals. The basic setup of this scheme is very

similar to the one described above, see Fig. 5. An ion of mass m, is trapped in a trap with frequency ω between coupling electrodes with effective distance D_{eff}. The parametric action in this case comes from the resonator capacitance which is variable. If the capacitance is modulated as $C = C_0\,(1 + \eta \sin(\nu\, t))$, with modulation index η at the difference frequency $\nu = \omega_{\text{LC}} - \omega$, the coupling strength, g, becomes time dependent, with modulation index η. Then, the parametric coupling strength which the authors of [16] derive becomes, in our notation, $\frac{1}{3}\eta\frac{\hbar\omega_{\text{LC}}e}{D_{\text{eff}}}\sqrt{\frac{Z_{\text{LC}}}{m\omega}}$.

In order to physically achieve the modulated capacitor with desired parameters, the authors propose using a microfabricated capacitor based on piezoelectric bulk acoustic wave (BAW) resonators. If one plate of the capacitor is constructed out of one side of a BAW responator, then by driving the resonator the capacitor spacing oscillates and the capacitance is modulated. As typical experimental parameters, the authors use a coil of inductance 440 nH, and total capacitance of the resonant circuit $C_0 \approx$46 fF, resonating at $2\pi \times 1$ GHz, and sinusoidally modulated at an index of 0.3. Then for a $^9\text{Be}^+$ ion with effective distance $D_{\text{eff}} = 100\,\mu$m and secular frequency $2\pi\times1$ MHz, the parametric coupling rate is $2\pi\times60$ kHz. With this coupling rate, the internal state of the ion and the state of the resonator can be swapped with fidelity higher than 95%. If this is realized, it will allow the toolbox of trapped-ion coherent control to be applied to the resonator. For example, as the authors discuss, non-classical states can be prepared in the resonant circuit by mapping states of the ion, different resonators can be entangled with each other, phase gates can be realized between distant ions, and quantum metrology of electromagnetic fields in the microwace regime become possible.

Potential challenges to implementing this type of experiment are operation of the ion trap and the piezoelectric resonator in a dilution refridgerator environment, which is required to achieve the high quality factor and low thermal occupation of the resonator modes. Additional problems can arise from off-resonant excitation of the resonator due to the (classical) parametric drive of the BAW at the frequency ν which is close to ω_{LC}. One important consideration here, is that the electrical signal induced by the ion has to be larger than $1/f$ charge noise in the pick-up electrodes. Such noise can arise from the surfaces of the coupling electrodes, and their intefaces with dielectric materials. The ion signal is of order $2 \times 10^{-4}\,e$. This is comparable, for instance, to the $1/f$ charge noise of a single electron transistor (SET), which optimized for small charge detection, at 1 MHz, over a bandwidth

of 100 kHz [97]. The value for charge noise at 1 MHz for a BAW is currently not known. One open question in this scheme is the possibility of extending the frequency range of BAW resonators to the several GHz range where state-of-the-art superconducting charge qubits currently operate.

C. Rydberg Atoms and Superconducting cQED

Here, atoms excited to high principal quantum number Rydberg states are each located above one coupling electrode, and the different electrodes are connected to each other, see Fig. 6 [39]. The connection can be made via a capacitive bus, or via a standing-wave transmission line resonator (cf. Sec. III). One significant advantage of this type of scheme is the large dipole moment of the atoms, which translates to high coupling strengths both for a capacititve and a resonant bus. Another important feature of this scheme is that typical transition frequencies between Rydberg states are in the microwave to millimeter wave regime. This implies high coupling strength to an electrical resonator bus, as discussed in section III. For the proposal of Sorensen *et al.* [39] a trapping height $h = 10\,\mu$m implies an effective distance $D_{\rm eff} \approx 14\,\mu$m and coupling rates $2\,\pi\times 3$ MHz, between the Rydberg states $|N = 49, s\rangle$, $|N = 50, p_{\rm z}\rangle$. The atoms can be seperated by distances of several millimeters.

Experimental efforts to construct superconducting atom trap chips, suitable for this type of experiment [98], as well as the first steps in observing the interaction of thermal beams of Rydberg atoms with coplanar waveguide resonators [99] are in progress (see Fig. 7). On the technical side, the most significant challenge in this type of scheme remains to reliably trap Rydberg atoms with long storage times at a distance of a few micrometers from electrode surfaces. This challenge can potentially be overcome by trapping Rydberg ions in radio-frequency traps, at the additional expense of using lower light wavelengths associated with Rydberg ion transitions. In addition, it is not known whether electronic noise arising from metallic and insulating materials in the vicinity of the atoms will be enhanced by the laser fields used for trapping and manipulating the atoms. Finally, frequencies above 10 GHz can make superconductor losses significant [100], while even higher frequencies limit the range of available superconducting materials. We note that more recent proposals have also considered quantum optics and quantum information applications which use the basic platform of Rydberg atoms in superconducting cQED architectures [101, 102]

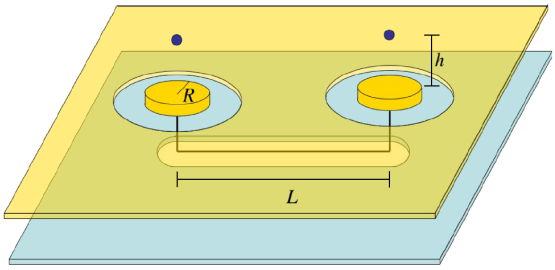

FIG. 6. Elementary geometry for coupling different Rydberg atoms, reproduced from [39]. Two cilyndrical electrodes of radius R are used to couple to Rydberg atoms, trapped at a height h above the electrode surface. The bus connecting the two electrodes can be superconducting, and can be covered underneath.

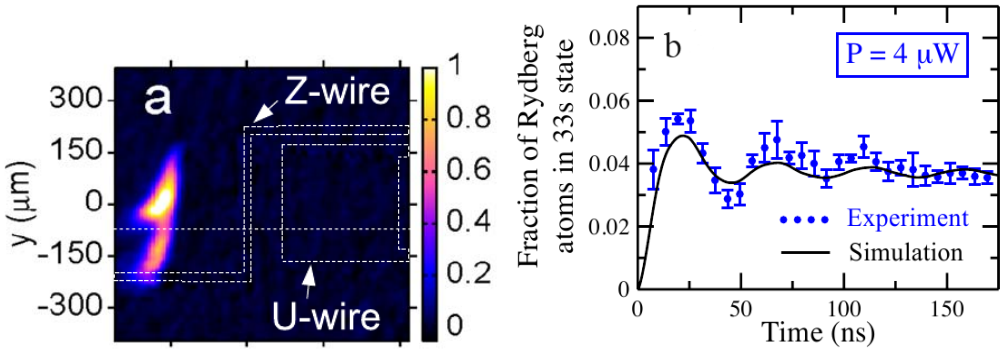

FIG. 7. (a) Absorption images of ^{87}Rb clouds trapped in a superconducting magnetic trap. The dashed lines outline the shape of the trap electrodes, the view is vertically from above the chip [98]. Atoms were trapped as close as 50 μm from the chip surface (b) Excitation of helium Rydberg atoms while in transit at a mean distance of 1 mm from a coplanar waveguide resonator. Oscillations of the population in the $|33, s\rangle$ state are visible. The coherence is limited by inhomogeneity in the electric fields arising from the resonator. Reproduced from [99].

D. Polar Atoms and Superconducting cQED

. Another possibility is to use cold polar molacules, coupled to electrical resonators [42, 43]. The resonators can be used as a quantum bus between polar molecules, or to couple molecules to superconducting charge qubits. Due to the lower dipole moment of polar molecules compared to Rydberg atoms, cf. Table I, the coupling to a resonator will be weaker. One way to increse the coupling is to use large ensembles of molecules [43]. For a cloud of 10^6 molecules, with dipole moment $\mu = 5$ D, trapped at an effective distance $D_{\rm eff} = 10\,\mu$m from a typical resonator, the coupling strength will be $g \approx 2\,\pi \times 10$ MHz. The

coherence of the Dicke states in which quantum information is encoded in the molecular cloud, can be limited by intermolecular collisions, and estimates on the strength of this effect put the decoherence rate at $\gamma \leq 4400\,\mathrm{s}^{-1}$ [43]. If individual molecules are used, significant coupling can only be achieved at submicron effective distance from the resonator. At an effective distance of $0.1\,\mu$m, CaBr with dipole moment of 4.36 D will couple to a 50 Ω transmission line with $g \approx 2\,\pi \times 400$ kHz [42].

For both Rydberg atoms and polar molecules trapped close to solid-state device surfaces, electric field noise arising from the surfaces will contribute to decoherence. Electric field noise at the atom (or molecule) transition frequency can drive transitions causing energy relaxation. White noise (e.g. Johnson) noise can be limited with appropriate setup design, but the anomalously large electric field noise encountered in ion trapping experiments was not included in previous estimates [42], and we evaluate its importance here. To estimate the strength of this effect, we take the typical measured electric field noise power spectral density, $S_E(\omega)$, near surfaces at cryogenic temperatures, which we mentioned in Sec II. This noise has been measured in the MHz range, and the extrapolation to the GHz regime introduces large uncertainty. For a Rydberg atom with $\mu \sim 5 \times 10^4$ D and transition frequency 5 GHz,at a distance of 10 μm from a solid surface, the damping rate will be $\gamma_1 \sim 5 - 25000\,\mathrm{s}^{-1}$, depending on whether the frequency scaling of the noise is $1/f$ or $1/f^2$. For a polar molecule with $\mu \sim 5$ D and transition frequency 5 GHz,at a distance of 0.1 μm from a solid surface, the damping rate will be in the same range, $\gamma_1 \sim 10 - 50000\,\mathrm{s}^{-1}$. Clearly the exponent of frequency scaling will be very important to the outcome of these experiments, and not much can be said before the actual measurements are performed.

Electric field noise will also contribute to dephasing of Rydberg atoms and polar molecules, due to static Stark shifts. In this case, the low frequency part of the electric field noise spectrum, over a bandwidth given by the coupling rate is relevant to dephasing. For Rydberg atoms, operation near a 'sweet-spot' where only quadratic Stark shifts occur, can be impractical [38]. In the absence of a sweet spot, the dephasing rate will be, up to a logarithmic factor, given by $\gamma_\varphi \sim \frac{\partial \omega}{\partial E} E_0$, where E_0 describes the strength of electric field noise $S_E = E_0^2/(f)^\alpha$, and $\frac{\partial \omega}{\partial E}$ is the sensitivity of the transition frequency to static fields. For Rydberg atoms trapped $10\,\mu$m from a solid surface the 'anomalous' noise seen in ion traps implies $\gamma_\varphi \sim 10^6\,\mathrm{s}^{-1}$. For polar molecules at a distance of 0.1 μm from a solid surface, operating near a 'sweet spot' the dephasing rate is $\gamma_\varphi \sim 600\,\mathrm{s}^{-1}$, using the parameters of

CaBr from [42]. Far from the sweet spot, the dephasing rate will also be $\gamma_\varphi > 10^6\,\mathrm{s}^{-1}$. It is clear that operation near a sweet spot is preferable for both Rydberg atoms and polar molecules. If this is not feasible, the dephasing problem can potentially be mitigated using dynamical decoupling schemes, but the details and compexity of such schemes remain to be evaluated.

E. Trapped Ion and Superconducting Charge Qubit

The electrostatic interaction of a trapped ion with a superconducting charge qubit can be used to implement a controlled phase gate between them, as proposed in [72, 103]. In this case, contrary to the above, no energy is exchanged between the two systems during the interaction. Rather, a $\sigma_z\,\sigma_z$ type interaction is used to imprint a state-dependent phase on the ion and the charge qubit. In specific, the ion is trapped near an electrically floated electrode, which is also capacitively coupled to the superconducting island of a charge qubit, as shown in Fig. 8. The electrode serves as a capacitive bus, shortening the effective distance between the ion and the charge qubit. Now, if the ion is displaced from its equilibrium position by x, or if the Cooper pair box contains one additional Cooper pair, described by σ_z, the electrostatic energy is increased by $\frac{e^2}{C}\,a\,\frac{x}{D_{\mathrm{eff}}}\,\sigma_z$. The capacitance C describes the capacitance of the coupling electrode to ground, and the factor a describes the relative voltage drop along a capacitive divider which supplies the ion signal to the superconducting island. If $C \approx 3$ fF, $x \sim 0.2\,\mu$m, $a \approx 0.5$, this interaction energy is approximately $\hbar\,2\,\pi \times$ 200 MHz. This interaction forms the basis of the phase gate, for example if a state-dependent displacement is applied to the ion, then the system will acquire a state-dependent phase π in $\tau_\pi \approx$2.5 ns. The phase is acquired only if both the ion is displaced, and the charge qubit has one additional Cooper pair. Two successive state-dependent laser kicks on the ion, in opposite directions and seperated by τ_π, then complete the phase gate. One additional feature is added to the scheme in order to increase the robustness of the charge qubit state to spurious signals present on the coupling electrode: the charge qubit is capacitively coupled to the wire via a switchable SQUID-based capacitive coupler [103].

The main advantage of this scheme is that it bypasses the frequency gap between a trapped ion signal and typical superconducting electronics. The main unresolved issue is that the fast phase gate operation relies on making the charge qubit very sensitive to the

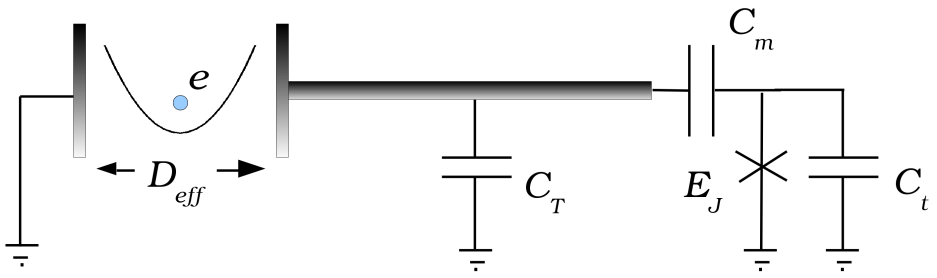

FIG. 8. An ion trapped next to a coupling electrode which is capacitively coupled to a superconducting charge qubit, as proposed in [72].

charge signal from the ion displacement, less than $10^{-2}e$ even if an ion displacement by 0.2 μm and a $D_{\rm eff} \approx 20\,\mu$m, are achieved. In practice this means, that one needs to keep the capacitance of the superconducting island to ground below the 1 fF range. This optimization is detrimental to the coherence of the charge qubit, as it becomes exceedingly sensitive to charge fluctuations of the environment nearby. The vast increases in charge qubit coherence times over the past decade, are to a large extent due to engineering the capacitance of the island to ground to be large [20].

Finally, we mention here that there are currently efforts to couple distant electrons in Penning traps [73] and distant ions [75] to each other via a capacitive bus. The coupling rates in these experiments follow from the general treatment of Sec. IV, but will not be derived here in detail. From the perspective of hybrid quantum devices, these experiments are important because they can provide insight into the decoherence mechanisms which are relevant to surface plasmon modes in metals, in the MHz frequency regime, and at the single quantum level.

F. Trapped Ion Coupled to Nanobeams

Tian *et al.* [91] discuss a single ion trapped in a Paul trap formed by two nanowires acting at the same time as nanomechanical oscillators. Radio frequency applied to these wires is supposed to confine the ions strongly such that they are resonant with the fundamental mechanical mode of the nanowries. As wires the authors propose carbon nanotubes with length of a few μm. The nanotubes are assumed to be spaced by 200 nm with an ion-tube distance of $d_0 = 100$ nm. The ion oscillates here at typical frequencies of $\omega = 2\pi \times 1$ GHz.

This results in a significant increase in the coupling strength, which turns out to be $g = \hbar\omega\sqrt{m_\mathrm{i}/m_\mathrm{b}} = 2\pi \times 10$ MHz.

The authors propose two experiments. In the first, quantum state engineering of entangled states of the form $|\Psi_1\rangle|\chi_2\rangle \pm |\chi_1\rangle|\Psi_2\rangle$ is considered, where the indices label two modes of the nanobeams with resonance frequencies differing by much more than the respective ion-beam couplings g_i. Secondly, the authors discuss also cooling a mode of the beams close to ground state by permantenly coupling the ion and beam while laser cooling the ion.

Despite the promising numbers, this type of experiment remains far from current capabilities of ion trap groups, as scaling ion trap fabrication technology to the nanoscale is a highly ambitious goal. Other difficulties may arise from the influence of the cooling lasers on the nanotube structure, the possibility of field ionization from the nanotubes, as well as electronic noise considerations are not estimated, and to a large extent cannot be estimated.

We finally turn our discussion to a similar system [92]. Here, the ion is assumed to be trapped by an electrode structure independent of the nanobeam. The nanobeam is charged to $Q = VC$, where $V \sim 10$ V is the voltage applied to the nanobeam and C is its capacitance. Neglecting image charges as well as the renormalization of the trap frequency (see Sec. IV), and using parameters for the nanobeam given in [104], the authors derive a coupling rate of $2\pi\times50$ kHz for coupling to a cadmium ion trapped at a distance of 50 μm from the nanobeam while estimating .

VII. SUMMARY

Quantum hybrid devices promise exciting opportunities both for fundamental physics and technology development. In particular, the quantum information and quantum sensing fields could benefit greatly from such a technology. We saw that various atomic systems and solid-state devices can provide platforms for hybrid systems, and summarized some common ways to interconnect them. The physical property considerations that go into the design of a hybrid device, can be summarized as follows:

A. Coupling Rate

For the qubits, a high dipole moment can be beneficial because it leads to increased coupling strength. For a harmonic oscillator, large (small) characteristic impedance implies strong coupling to electric (magnetic) dipoles. Intermediate values of characteristic impedance can be optimal for a harmonic oscillator bus used to couple an electric dipole to a magnetic dipole. For a capacitive bus, small capacitance to ground and large coupling to the electric dipoles (i.e. large electric fields at the dipoles) are required. The different scales and technological operation requirements of atoms and solid state systems can be seen as a vast impedance mismatch, on the order of ten orders of magnitude. This gap can be partially bridged by a well engineered quantum bus or simply by increasing the number of atoms to couple to.

B. Coherence Time

Long coherence times are required for both of the qubits and the bus in a hybrid. As a rule of thumb, the sum of all decoherence rates in the hybrid should be much smaller than the lowest coupling rate between different components. Minimizing thermal noise can usually be achieved by minimizing blackbody radiation at the bandwidth of interest, for example ~ 5 GHz signals at ~ 50 mK temperatures. To minimize non-thermal sources of decoherence, we are required to understand the physical environment of all the components of our device, i.e. identify what environmental degrees of freedom are relevant, and how strongly they couple to the dipoles or the electromagnetic field of a resonator. Both the solid state qubit, the atomic qubit, and the electromagnetic field of the bus must couple to each other more strongly than to all other degrees of freedom in the environment. A perhaps physically more transparent way to say this, is that the quantum signals transmitted by the bus have to be much stronger than the environmental noise injected to the qubits over the the bandwidth of the bus. Therefore it is useful to limit the bandwidth of the bus to the coupling rate in order to filter unwanted sources of decoherence.

C. System Compatibility

The operation of each component of a hybrid should interfere as little as possible with the rest. The atoms should be reliably trapable, preferably with long storage times, in the presence of the solid state environment, with minimal interference. This is a two-fold requirement. On one side, optical, radio-frequency, and static electromagnetic fields used for trapping and manipulating the atoms should interfere minimally with the solid-state devices. The possible effects range from thermal load management, to decoherence induced by the strong fields required for the atomic system. On the other side, the presence of the solid state environment and the control fields used for the solid-state qubit operation, should cause minimal decoherence to the atoms. Additional compatibility requirements arise if the atomic system and the solid-state system cannot be made resonant with each other. In these cases, a non-linear coupling mechanism can be used to implement a parametric frequency conversion scheme between the two sides. Alternatively, a dispersive coupling scheme can provide phase-gate (i.e. $\sigma_z \otimes \sigma_z$) type coupling. In both cases, increased sensitivity to noise, as well as noise added because of the interface have to be carefully evaluated.

VIII. CONCLUSIONS

We identify the large intrinsic decoherence of solid-state systems in combination with the small dipole moments of atomic systems (with the exception of Rydberg atoms) as the main challenge toward interfacing atomic with solid-state systems. We envision devices in which quantum in- formation flows from one side to the other. At the end of this endeavor could be quantum in- formation–processing devices with an atomic memory and a solid state–based processing unit. Mastering the technological challenges will provide us also with unique means to probe quantum effects in the solid state. Thus, we can hope to take advantage of the quantum control and long coherence times of trapped atomic systems to probe the complex and strongly correlated quantum–many body states in the solid state.

[1] Rainer Blatt and David Wineland. Entangled states of trapped atomic ions. *Nature*, 453(7198):1008–15, June 2008.

[2] H. Häffner, C. F. Roos, and R. Blatt. Quantum computing with trap ions. *Physics Reports*, 469:155, 2008.

[3] Immanuel Bloch, Jean Dalibard, and Sylvain Nascimbène. Quantum simulations with ultracold quantum gases. *Nature Physics*, 8:267, 2012.

[4] John Clarke and Frank K Wilhelm. Superconducting quantum bits. *Nature*, 453:1031–1042, 2008.

[5] R J Schoelkopf and S M Girvin. Wiring up quantum systems. *Nature*, 451(7179):664–669, February 2008.

[6] Steven M Girvin. Superconducting Qubits and Circuits : Artificial Atoms Coupled to Microwave Photons. *Lecture notes, Les Houches, Oxford University Press*, (July), 2011.

[7] Hanhee Paik, D. Schuster, Lev Bishop, G. Kirchmair, G. Catelani, A. Sears, B. Johnson, M. Reagor, L. Frunzio, L. Glazman, S. Girvin, M. Devoret, and R. Schoelkopf. Observation of High Coherence in Josephson Junction Qubits Measured in a Three-Dimensional Circuit QED Architecture. *Physical Review Letters*, 107:240501, December 2011.

[8] Chad Rigetti, Stefano Poletto, Jay M Gambetta, B L T Plourde, Jerry M Chow, A John, Seth T Merkel, J R Rozen, George A Keefe, Mary B Rothwell, Mark B Ketchen, and M Steffen. Superconducting qubit in waveguide cavity with coherence time approaching 0.1ms. *arXiv:1202.5533v1*, pages 1–4.

[9] D. Hunger, S. Camerer, M. Korppi, a. Jöckel, T.W. Hänsch, and P. Treutlein. Coupling ultracold atoms to mechanical oscillators. *Comptes Rendus Physique*, 12(9-10):871–887, December 2011.

[10] A O Caldeira and A J Leggett. Quantum tunneling in a dissipative system. *Annals of Physics*, 149:374–456, November 1983.

[11] A. J. Leggett. Testing the limits of quantum mechanics : motivation , state of play , prospects. *Journal of Physics: Condensed Matter*, 14:415, 2002.

[12] Wojciech Hubert Zurek. Decoherence, einselection, and the quantum origins of the classical. *Reviews of Modern Physics*, 75(3):715–775, May 2003.

[13] JJ Bollinger, DJ Heinzen, WM Itano, SL Gilbert, and DJ Wineland. A 303-MHz frequency standard based on trapped Be+ ions. *IEEE transactions on instrumentation and measurement*, 40(2):126–128, 1991.

[14] P T H Fisk, M J Sellars, M A Lawn, and C Coles. Accurate measurement of the 12.6 GHz Clock transition in trapped $ˆ{171}$Yb$ˆ+$ ions. *IEEE Trans. Ultrason. Ferroelectr. Freq. Control*, 44:344, 1997.

[15] D J Heinzen and D J Wineland. Quantum-limited Cooling and Detection of Radio-Frequency Oscillations by Laser-cooled Ions. *Phys. Rev. A*, 42:2977, 1990.

[16] D. Kielpinski, D. Kafri, M. Woolley, G. Milburn, and J. Taylor. Quantum Interface between an Electrical Circuit and a Single Atom. *Physical Review Letters*, 108(13):130504, March 2012.

[17] A. Wallraff, DI Schuster, A. Blais, L. Frunzio, R.S. Huang, J. Majer, S. Kumar, SM Girvin, and RJ Schoelkopf. Strong coupling of a single photon to a superconducting qubit using circuit quantum electrodynamics. *Nature*, 431(7005):162–166, 2004.

[18] Alexandre Blais, Ren-Shou Huang, Andreas Wallraff, S. Girvin, and R. Schoelkopf. Cavity quantum electrodynamics for superconducting electrical circuits: An architecture for quantum computation. *Physical Review A*, 69(6):062320, June 2004.

[19] M H Devoret, A Wallraff, and J M Martinis. Superconducting Qubits : A Short Review. *arXiv:cond-mat/0411174v1*, 2008.

[20] Jens Koch, Terri Yu, Jay Gambetta, A. Houck, D. Schuster, J. Majer, Alexandre Blais, M. Devoret, S. Girvin, and R. Schoelkopf. Charge-insensitive qubit design derived from the Cooper pair box. *Physical Review A*, 76(4):042319, October 2007.

[21] Z. Kim, B. Suri, V. Zaretskey, S. Novikov, K. Osborn, A. Mizel, F. Wellstood, and B. Palmer. Decoupling a Cooper-Pair Box to Enhance the Lifetime to 0.2 ms. *Physical Review Letters*, 106(12):120501, March 2011.

[22] D I Schuster, A A Houck, J A Schreier, A Wallraff, J M Gambetta, A Blais, L Frunzio, J Majer, B Johnson, M H Devoret, S M Girvin, and R J Schoelkopf. Resolving photon number states in a superconducting circuit. *Nature*, 445:515–518, 2007.

[23] F. Yoshihara, K. Harrabi, a. Niskanen, Y. Nakamura, and J. Tsai. Decoherence of Flux Qubits due to 1/f Flux Noise. *Physical Review Letters*, 97(16):1–4, October 2006.

[24] Jr Friedman, V Patel, W Chen, Sk Tolpygo, and Je Lukens. Quantum superposition of distinct macroscopic states. *Nature*, 406(6791):43–6, July 2000.

[25] T Lindström, C H Webster, J E Healey, M S Colclough, C M Muirhead, and a Ya Tzalenchuk. Circuit QED with a flux qubit strongly coupled to a coplanar transmission line resonator. *Superconductor Science and Technology*, 20(8):814–821, August 2007.

[26] S M Anton, C Miller, J S Birenbaum, S R O Kelley, A D Fefferman, D S Golubev, H Cho, K D Irwin, F C Wellstood, Gerd Sch, A Shnirman, and John Clarke. Pure dephasing in flux qubits due to flux noise with spectral density scaling as 1/f. *arXiv:1111.7272v2*, pages 1–7.

[27] John M. Martinis. Superconducting phase qubits. *Quantum Information Processing*, 8(2-3):81–103, February 2009.

[28] D P McGinnis and J B Beyer. A Broad-Band Microwave Superconducting. *IEEE Trans. Microwave Th. Techn.*, 36(11):1521–1525, 1988.

[29] Henry G. Leduc, Bruce Bumble, Peter K. Day, Byeong Ho Eom, Jiansong Gao, Sunil Golwala, Benjamin a. Mazin, Sean McHugh, Andrew Merrill, David C. Moore, Omid Noroozian, Anthony D. Turner, and Jonas Zmuidzinas. Titanium nitride films for ultrasensitive microresonator detectors. *Applied Physics Letters*, 97(10):102509, 2010.

[30] Jiansong Gao, Jonas Zmuidzinas, Benjamin a. Mazin, Henry G. LeDuc, and Peter K. Day. Noise properties of superconducting coplanar waveguide microwave resonators. *Applied Physics Letters*, 90(10):102507, 2007.

[31] Jiansong Gao, Miguel Daal, Anastasios Vayonakis, Shwetank Kumar, Jonas Zmuidzinas, Bernard Sadoulet, Benjamin a. Mazin, Peter K. Day, and Henry G. Leduc. Experimental evidence for a surface distribution of two-level systems in superconducting lithographed microwave resonators. *Applied Physics Letters*, 92(15):152505, 2008.

[32] Shwetank Kumar, Jiansong Gao, Jonas Zmuidzinas, Benjamin A. Mazin, Henry G. LeDuc, and Peter K. Day. Temperature dependence of the frequency and noise of superconducting coplanar waveguide resonators. *Applied Physics Letters*, 92(12):123503, 2008.

[33] H. Wang, M. Hofheinz, J. Wenner, M. Ansmann, R. C. Bialczak, M. Lenander, Erik Lucero, M. Neeley, a. D. O'Connell, D. Sank, M. Weides, a. N. Cleland, and John M. Martinis. Improving the coherence time of superconducting coplanar resonators. *Applied Physics Letters*, 95(23):233508, 2009.

[34] M R Vissers, J Gao, D S Wisbey, D A Hite, A D Corcoles, M Steffen, D P Pappas, and Yorktown Heights. Low Loss Superconducting Titanium Nitride Coplanar Waveguide Resonators. (100):1–13.

[35] A Megrant, C Neill, R Barends, B Chiaro, Yu Chen, L Feigl, J Kelly, Erik Lucero, Matteo Mariantoni, P J J O Malley, D Sank, A Vainsencher, J Wenner, T C White, Y Yin, J Zhao, C J Palmstrø m, and John M Martinis. Planar superconducting resonators with internal quality factors above one million. *Applied Physics Letters*, 113510:11–14, 2012.

[36] K. Geerlings, S. Shankar, E. Edwards, L. Frunzio, R. J. Schoelkopf, and M. H. Devoret. Improving the quality factor of microwave compact resonators by optimizing their geometrical parameters. *Applied Physics Letters*, 100(19):192601, 2012.

[37] S. Kuhr, S. Gleyzes, C. Guerlin, J. Bernu, U. B. Hoff, S. Del\'eglise, S. Osnaghi, M. Brune, J.-M. Raimond, S. Haroche, E. Jacques, P. Bosland, and B. Visentin. Ultrahigh finesse Fabry-P\'erot superconducting resonator. *Applied Physics Letters*, 90(16):164101, 2007.

[38] M. Saffman, T. Walker, and K. Mø lmer. Quantum information with Rydberg atoms. *Reviews of Modern Physics*, 82(3):2313–2363, August 2010.

[39] A.S. Sø rensen, C.H. van Der Wal, L.I. Childress, and M.D. Lukin. Capacitive coupling of atomic systems to mesoscopic conductors. *Phys. Rev. Lett.*, 92(6):63601, 2004.

[40] X. Maître, E. Hagley, G. Nogues, C. Wunderlich, P. Goy, M. Brune, J. M. Raimond, and S. Haroche. Quantum Memory with a Single Photon in a Cavity. *Physical Review Letters*, 79(4):769–772, July 1997.

[41] D DeMille. Quantum Computation with Trapped Polar Molecules. *Phys. Rev. Lett.*, 88:67901, 2002.

[42] A. André, D. DeMille, J. M. Doyle, M. D. Lukin, S. E. Maxwell, P. Rabl, R. J. Schoelkopf, and P. Zoller. A coherent all-electrical interface between polar molecules and mesoscopic superconducting resonators. *Nature Physics*, 2(9):636–642, August 2006.

[43] P Rabl, D DeMille, J M Doyle, M D Lukin, R J Schoelkopf, and P Zoller. Hybrid quantum processors: molecular ensembles as quantum memory for solid state circuits. *Phys Rev Lett*, 97:33003, July 2006.

[44] D. Leibfried, R. Blatt, C. Monroe, and D. Wineland. Quantum dynamics of single trapped ions. *Rev. Mod. Phys.*, 75(1):281–324, 2003.

[45] K R Brown, C Ospelkaus, Y Colombe, a C Wilson, D Leibfried, and D J Wineland. Coupled quantized mechanical oscillators. *Nature*, 471(7337):196–9, March 2011.

[46] Ch. Roos, Th. Zeiger, H Rohde, H C Nägerl, J Eschner, D Leibfried, F Schmidt-Kaler, and R Blatt. Quantum state engineering on an optical transition and decoherence in a Paul trap. *Physical Review Letters*, 83:4713, 1999.

[47] D J Wineland, C Monroe, W M Itano, D Leibfried, B E King, and D M Meekhof. Experimental Issues in Coherent Quantum-State Manipulation of Trapped Atomic Ions. *Journal of Research of the National Institute for Standards and Technology*, 103:259–328, 1998.

[48] Nikos Daniilidis and Hartmut Häffner. All that is gold does not glitter. *Physics*, 4:9–11, August 2011.

[49] L Deslauriers, P C Haljan, P J Lee, K.-A. Brickman, B B Blinov, M J Madsen, and C Monroe. Zero-point cooling and low heating of trapped $ˆ{111}$Cd$ˆ+$ ions. *Physical Review A*, 70:43408, 2004.

[50] Jaroslaw Labaziewicz, Yufei Ge, David Leibrandt, Shannon X Wang, Ruth Shewmon, and Isaac L Chuang. Temperature Dependence of Electric Field Noise Above Gold Surfaces. *Physical Review Letters*, 101:180602, 2008.

[51] A. Safavi-Naini, P. Rabl, P. Weck, and H. Sadeghpour. Microscopic model of electric-field-noise heating in ion traps. *Phys. Rev. A*, 84:023412, 2011.

[52] D A Hite, Y Colombe, A C Wilson, K R Brown, U Warring, J D Jost, D P Pappas, D Leibfried, and D J Wineland. Reduction of anomalous heating in an in-situ-cleaned ion trap. *arXiv:1112.5419v1*, pages 1–7.

[53] Ying-Ju Wang, Matthew Eardley, Svenja Knappe, John Moreland, Leo Hollberg, and John Kitching. Magnetic Resonance in an Atomic Vapor Excited by a Mechanical Resonator. *Physical Review Letters*, 97:227602, December 2006.

[54] J. Suh, M.D. LaHaye, P. Echternach, K.C. Schwab, and M.L. Roukes. Parametric Amplification and back-action noise squeezing by a qubit-coupled nanomechanical resonator. *Nano Letters*, 10:3990–3994, 2010.

[55] B. M. Zwickl, W. E. Shanks, a. M. Jayich, C. Yang, a. C. Bleszynski Jayich, J. D. Thompson, and J. G. E. Harris. High quality mechanical and optical properties of commercial silicon nitride membranes. *Applied Physics Letters*, 92(10):103125, 2008.

[56] Scott S. Verbridge, Harold G. Craighead, and Jeevak M. Parpia. A megahertz nanomechanical resonator with room temperature quality factor over a million. *Applied Physics Letters*, 92(1):013112, 2008.

[57] O. Arcizet, R. Rivière, a. Schliesser, G. Anetsberger, and T. Kippenberg. Cryogenic properties of optomechanical silica microcavities. *Physical Review A*, 80(2):1–4, August 2009.

[58] P. Rabl, P. Cappellaro, M. V. Gurudev Dutt, L. Jiang, J. R. Maze, and M. D. Lukin. Strong magnetic coupling between an electronic spin qubit and a mechanical resonator. *Physical Review B (Condensed Matter and Materials Physics)*, 79(4):041302–4, January 2009.

[59] Swati Singh and Pierre Meystre. Atomic probe Wigner tomography of a nanomechanical system. *Physical Review A*, 81:041804(R), April 2010.

[60] D Marcos, M Wubs, J M Taylor, R Aguado, M D Lukin, and A S Sø rensen. Coupling Nitrogen-Vacancy Centers in Diamond to Superconducting Flux Qubits. 105(November):210501, 2010.

[61] Guozhu Sun, Zhongyuan Zhou, Bo Mao, Xueda Wen, Peiheng Wu, and Siyuan Han. Entanglement Dynamics of a Coupled Phase Qubit-TLS System. *arXiv:1111.3016v2*, pages 1–6, 2011.

[62] Y Kubo, I Diniz, A Dewes, V Jacques, A Auffeves, D Vion, D Esteve, and P Bertet. Storage and Retrieval of a Microwave Field in a Spin Ensemble. *arXiv:1109.3960v1*, pages 1–8, 2011.

[63] Gopalakrishnan Balasubramanian, Philipp Neumann, Daniel Twitchen, Matthew Markham, Roman Kolesov, Norikazu Mizuochi, Junichi Isoya, Jocelyn Achard, Johannes Beck, Julia Tissler, Vincent Jacques, Philip R Hemmer, Fedor Jelezko, and Jörg Wrachtrup. Ultralong spin coherence time in isotopically engineered diamond. *Nature materials*, 8(5):383–7, May 2009.

[64] Jonas Bylander, Simon Gustavsson, Fei Yan, Fumiki Yoshihara, Khalil Harrabi, George Fitch, David G. Cory, Yasunobu Nakamura, Jaw-Shen Tsai, and William D. Oliver. Noise spectroscopy through dynamical decoupling with a superconducting flux qubit. *Nature Physics*, 7(7):565–570, May 2011.

[65] Katarina Cicak, Dale Li, Joshua a. Strong, Michael S. Allman, Fabio Altomare, Adam J. Sirois, Jed D. Whittaker, John D. Teufel, and Raymond W. Simmonds. Low-loss superconducting resonant circuits using vacuum-gap-based microwave components. *Applied Physics Letters*, 96(9):093502, 2010.

[66] C. P. Slichter. *Principles of Magnetic Resonance*. Springer-Verlag, 1978.

[67] M Harlander, R Lechner, M Brownnutt, R Blatt, and W Hänsel. Trapped-ion antennae for the transmission of quantum information. *Nature*, 471(7337):200–3, March 2011.

[68] G S Agarwal. Quantum Statistical Theories of Spontaneous Emission and their Relation to Other Approaches. *Springer Tracts in Quantum Optics*, 70:1–128, 1974.

[69] M A Nielsen and I L Chuang. *Quantum Computation and Quantum Information*. Cambridge Univ. Press, Cambridge, 2000.

[70] A Sø rensen and K Mø lmer. Entanglement and quantum computation with ions in thermal motion. *Phys. ˜Rev. ˜A*, 62:22311, 2000.

[71] C F Roos. Ion trap quantum gates with amplitude-modulated laser beams. *New J. Phys.*, 10:13002, 2008.

[72] L Tian, P Rabl, R Blatt, and P Zoller. Interfacing quantum-optical and solid-state qubits. *Physical Review Letters*, 92(24):247902, June 2004.

[73] S Stahl, F Galve, J Alonso, S Djekic, W Quint, T Valenzuela, J Verdú, M Vogel, and G Werth. A planar Penning trap. *Eur. Phys. J. D*, 32:139, 2005.

[74] Jorge R Zurita-Sánchez and Carsten Henkel. Wiring up single electron traps to perform quantum gates. *New Journal of Physics*, 10(8):083021, August 2008.

[75] N Daniilidis, T Lee, R Clark, S Narayanan, and H Häffner. Wiring up trapped ions to study aspects of quantum information. *J. Phys. B*, 42:154012, 2009.

[76] P. Rabl, S. J. Kolkowitz, F. H. L. Koppens, J. G. E. Harris, P. Zoller, and M. D. Lukin. A quantum spin transducer based on nanoelectromechanical resonator arrays. *Nature Physics*, 6(8):602–608, May 2010.

[77] W.H. Louisell, A. Yariv, and A.E. Siegman. Quantum Fluctuations and Noise in Parametric Processes. I. *Physical Review*, 124(1961):1646, 1961.

[78] W.H. Louisell. *Quantum Statistical Properties of Radiation*. Wiley and Sons, 1973.

[79] Michel H Devoret. Quantum Fluctuations in Electrical Circuits. In S Reynaud, E. Giacobino, and J. Zinn-Justin, editors, *Les Houches, Session LXIII, 1995, Quantum Fluctuations*. Elsevier, 1997.

[80] W Shockley. Currents to conductors induced by a moving point charge. *J. App. Phys.*, 9:635, 1938.

[81] D J Wineland and H G Dehmelt. Principles of the stored ion calorimeter. *J. App. Phys.*, 46:919, 1975.

[82] B Yurke and J S Denker. Quantum network theory. *Physical Review A*, 29(3):1419, 1984.

[83] M. G\"oppl, A. Fragner, M. Baur, R. Bianchetti, S. Filipp, J. M. Fink, P. J. Leek, G. Puebla, L. Steffen, and A. Wallraff. Coplanar waveguide resonators for circuit quantum electrodynamics. *Journal of Applied Physics*, 104(11):113904, 2008.

[84] Interestingly, for the typical dipole values $ea_0/2$ and μ_B used before, and when the effective distances are equal, the optinal impedance turns out to be the resistance quantum $\alpha Z_0 = 2\pi\hbar/e^2 \approx 25.8\,\mathrm{k}\Omega$.

[85] T J Kippenberg and K J Vahala. Cavity optomechanics: back-action at the mesoscale. *Science (New York, N.Y.)*, 321(5893):1172–6, August 2008.

[86] D Gorman and I Hayes. private communication.

[87] N Daniilidis, S Narayanan, S Möller, R Clark, T Lee, P Leek, A Wallraff, St Schulz, F Schmidt-Kaler, and H Häffner. Fabrication and heating-rate study of microscopic surface electrode traps. *New J. Phys.*, 13:013032, 2011.

[88] D. F. Walls and G. J. Milburn. Effect of dissipation on quantum coherence. *Phys Rev A*, 31:2403, 1985.

[89] A. M. Nielsen and I L Chuang. *Quantum Computation and Quantum Information*. Cambridge Univ. Press, Cambridge, 2000.

[90] J R Johansson, P D Nation, and Franco Nori. QuTiP: An open-source Python framework for the dynamics of open quantum systems. *arXiv:1110.0573v2*, 2011.

[91] L Tian and P Zoller. Coupled ion-nanomechanical systems. *Phys. Rev. Lett.*, 93(26 Pt 1):266403, December 2004.

[92] W K Hensinger, D Wahyu Utami, H.-S. Goan, K Schwab, C Monroe, and G J Milburn. Ion trap transducers for quantum electromechanical oscillators. *Phys. Rev. A*, 72:041405(R), 2005.

[93] L.S. Brown and G. Gabrielse. Geonium theory: Physics of a single electron or ion in a Penning trap. *Reviews of Modern Physics*, 58(1):233–311, 1986.

[94] M Weisskoff, G P Lafyatis, E A Corneli, and D E Pritchard. rf SQUID detector for single ion trapping experiments. *Journal of Applied Physics*, 63(May):4599–4604, 1988.

[95] It is useful to write the ion equivalent impedance, as seen from the circuit, as $Z_{\text{ion}} = \frac{\hbar D_{\text{eff}}^2}{2\mu_{\text{ion}}^2}$. This allows us to assign an equivalent circuit impedance to electrical dipoles in general.

[96] S Ulmer, H Kracke, K Blaum, S Kreim, a Mooser, W Quint, C C Rodegheri, and J Walz. The quality factor of a superconducting rf resonator in a magnetic field. *The Review of scientific instruments*, 80(12):123302, December 2009.

[97] Yu. a. Pashkin, O. Astafiev, T. Yamamoto, Y. Nakamura, and J. S. Tsai. Josephson charge qubits: a brief review. *Quantum Information Processing*, 8(2-3):55–80, February 2009.

[98] A. Emmert, A. Lupaşcu, M. Brune, J.-M. Raimond, S. Haroche, and G. Nogues. Microtraps for neutral atoms using superconducting structures in the critical state. *Physical Review A*, 80(6), 2009.

[99] S. Hogan, J. Agner, F. Merkt, T. Thiele, S. Filipp, and A. Wallraff. Driving Rydberg-Rydberg Transitions from a Coplanar Microwave Waveguide. *Physical Review Letters*, 108(6):063004, February 2012.

[100] T Van Duzer and C W Turner. *Principles of Superconductive Devices and Circuits*. 1981.

[101] David Petrosyan and Michael Fleischhauer. Quantum Information Processing with Single Photons and Atomic Ensembles in Microwave Coplanar Waveguide Resonators. *Physical Review Letters*, 100:170501, April 2008.

[102] David Petrosyan, Guy Bensky, Gershon Kurizki, Igor Mazets, Johannes Majer, and Jörg Schmiedmayer. Reversible state transfer between superconducting qubits and atomic ensembles. *Physical Review A*, 79(4):040304(R), April 2009.

[103] L Tian, R Blatt, and P Zoller. Scalable ion trap quantum computing without moving ions. *Eur. Phys. J. D*, 32:201, 2005.

[104] M D LaHaye, O Buu, B Camarota, and K C Schwab. Approaching the quantum limit of a nanomechanical resonator. *Science (New York, N.Y.)*, 304(5667):74–7, April 2004.